PCCP

Accepted Manuscript

ROYAL SOCIETY OF CHEMISTRY

www.rsc.org/pccp

Regulation of Nonadiabatic Processes in Photolysis of Some Carbonyl Compounds

King-Chuen Lin

Department of Chemistry, National Taiwan University, Taipei 106, and Institute of Atomic and Molecular Sciences, Academia Sinica, Taipei 106, Taiwan

Pages: 61

Figures: 15

Email address: kclin@ntu.edu.tw

Table of contents

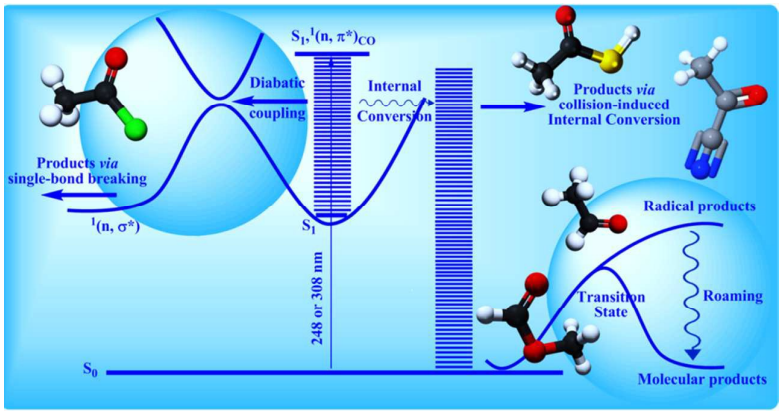

Energy scheme involving $S_o \rightarrow S_1$ excitation, followed by dissociation channels via diabatic coupling, internal conversion, transition state and roaming mechanism.

Abstract

Carbonyl compounds studied are confined to acetyl halides (CH_3COCl), acetyl cyanide (CH3COCN), acetyl sulfide (CH3COSH), acetaldehyde (CH_3CHO), and methyl formate ($HCOOCH_3$). They are asymmetrically substituted, but do not follow the well-known Norrish type I reactions. Each compound ejected in an effusive beam at about 300 K is commonly excited to the $^1(n, \pi^*)_{CO}$ lower state; that is, a nonbonding electron on O of C=O group is promoted to the antibonding orbital of π^*_{CO}. The photolysis experiments are conducted in the presence of Ar gas and the corresponding fragments are detected using time-resolved Fourier-transform Infrared (FTIR) emission spectroscopy. The enhancement of the collision-induced internal conversion or intersystem crossing facilitates the dissociation channels via highly vibrational states of the ground singlet (S_o) or triplet (T_1) potential energy surfaces. In this manner, an alternative nonadiabatic channel is likely open yielding different products, even if the diabatic coupling strength is strong between the excited state and the neighboring state. For instance, photodissociation of CH_3COCl at 248 nm produces HCl, CO, and CH_2 fragments, in contrast to the supersonic jet experiments showing dominance of Cl fragment eliminated from the excited state. If the diabatic coupling strength is weak, the dissociation proceeds mainly through internal conversion, such as the cases of CH_3COCN and CH_3COSH. The photodissociation of CH_3COCN at 308 nm has never been reported before, while the CH_3COSH was conducted by matrix-isolated photodissociation that shows distinct spectral feature from the current FTIR method. The CH_3CHO and $HCOOCH_3$ molecules belong to the same type of carbonyl compounds, in which the molecular products, $CO+CH_4$ and $CO+CH_3OH$, are produced

through both transition state and roaming pathways. Their products are characterized differently between molecular beam and current FTIR experiments. For instance, photodissociation of $HCOOCH_3$ at 248 nm yields CO with vibrational state v≥ 4, in contrast to the molecular beam experiments producing CO at v=1. Photodissociation of CH_3CHO at 308 nm intensifies a low energy component in CH_4 vibrational distribution, thus verifying the transition state pathway for the first time.

1. Introduction

Carbonyl compounds (RCOR') (R=H or alkyl, R'=H, alkyl or other functional groups) form a very important class of organic compounds. For instance, aliphatic aldehydes RCOH are generated in the atmosphere through biogenic and anthropogenic emissions and through photo-oxidation of tropospheric organic compounds. They play a vital role in the formation of photochemical smog, peroxyacetyl nitrate (PAN), and ground-level ozone.[1,2] Acyl halides RCOX (X: halogen atom) are another example that can release halogen atoms after decomposition, thus causing potential threat to stratospheric ozone and environmental issue.[3] Photodissociation and reaction with OH radical are known to be the major pathways to remove these polluted sources. Between them, the UV photodissociation process is verified to be more efficient to shorten their lifetimes in the atmosphere.[4]

In this review, we confine carbonyl compounds studied to acetyl halides (CH_3COCl), acetyl cyanide (CH3COCN), acetyl sulfide (CH3COSH), acetaldehyde (CH_3CHO), and methyl formate ($HCOOCH_3$). They all belong to asymmetrically substituted carbonyl compounds, but do not follow the well-known Norrish type I reactions, among which the weaker C–C α bond may be cleaved preferentially as a result of rapid internal vibrational redistribution.[5] For instance, the dissociation of acyl chlorides (RCOCl) is dominated by the C–Cl bond rupture in gas phase,[6-9] showing a feature of nonstatistical reaction. Acetyl cyanide, CH_3COCN, is another example, undergoing the following competing dissociation reactions, upon irradiation by UV light:[10-14]

$$CH_3COCN \rightarrow CH_3CO + CN, \qquad (1)$$

$CH_3COCN \rightarrow CH_3 + COCN.$ (2)

Due to partial double bond conjugation, the C-CN bond cleavage should be much harder than the other C-CH_3 bond if the reaction is statistical. However, the branching ratios between eq.1 and 2 were reported to consistently favor the CN elimination in the photolysis at 193 nm.[10-14]

By adjusting the UV photolysis wavelength, the carbonyl compounds may be selected to the $^1(n, \pi^*)_{CO}$ lower state that is likely to undergo diabatic interaction with the neighboring $^1(n, \sigma^*)$ state to cause the adjacent single bond rupture, if the coupling strength is large. In the photodissociation of acetyl chloride at 248 nm, the C-Cl bond broke rapidly through the diabatic interaction with $^1(n_{Cl}, \sigma_{C-Cl}^*)$ repulsive configuration.[7-9] In contrast, the $S_1(A'')$, $^1(n_O, \pi^*_{CO})$ state of CH_3COCN, with a longer lifetime about 3.5±0.3 μs from ~ 338 to 363.5 nm,[15] reduces substantially the possibility of fast vibrational and electronic predissociation processes. The CN or CH_3 products, reported as the major channel at 193 nm,[10-14] may not be eliminated efficiently. Instead, alternative product channels exist.[16] It is thus worthwhile to systematically look into variation of the photodissociation products for these carbonyl compounds selected, when the photolysis wavelength is confined to promote the nonbonding electron on O of C=O group to the antibonding orbital of π^*_{CO}.

Further, even if the above diabatic coupling is strong, an alternative nonadiabatic channel is likely open yielding different products by controlling the experimental conditions. In the 248 nm photolysis of C_2H_5COCl molecular beam under jet-cooled temperature, the Cl (Cl*) elimination was found to dominate over the dissociation products.[17] However, when the nozzle of molecular beam was heated to 153 ^oC,[18] the major fast dissociation channel of C–Cl bond fission was accompanied by a minor channel of HCl elimination which proceeded on the

ground state. When the photodissociation was conducted under the matrix-isolation condition, $CH_3CH=CO\cdots HCl$ complex was the only product, in which HCl was situated perpendicular to the carbonyl group of methyl ketene. The HCl molecule was generated by four-center elimination of the ground state molecule via internal conversion (IC).[19]

Therefore, to find out the possibility of regulating nonadiabatic product channels for the carbonyl compounds is of interest, but challenging, especially under the condition of a strong diabatic coupling with the neighboring state. In this article, we take advantage of the phenomena of collision-induced IC or intersystem crossing (ISC) that facilitate the dissociation channels proceeding on the ground state or triplet state surfaces. Following photodissociation of each carbonyl compound in a thermally equilibrated (~300 K) sample in the presence of a few Torr of background gas (Ar or sometimes O_2), the resulting fragments are detected using time-resolved Fourier-transformed infrared (FTIR) emission spectroscopy. In this manner, we find the obtained dissociation channels different from those under supersonic jet condition. Even if the products are the same, they are characterized with different internal energy disposals. The detailed dissociation pathway for each carbonyl compound will be discussed with the aid of theoretical calculations.

2. Experimental

2.1. Time-resolved FTIR emission spectroscopy

The apparatus, employed throughout all the experiments for the above carbonyl compounds, contains a step-scan FTIR emission spectroscopy for spectral detection of the fragments and a six-way stainless steel cube as reaction

chamber in which a multi-pass optical system is housed.[16,20-22] The multi-pass optical system, composed of two pairs of 2"-diameter gold-coated curved mirrors and positioned perpendicular to the laser propagation direction, was used to enhance the IR emission signal-to-noise ratio.

A ~20 ns, 10 Hz, photolysis laser emitting at 248 or 308 nm was controlled in the energy range of 6 - 85 mJ/pulse prior to focusing with a spherical lens to a beam size of 4×2 mm^2. The focused radiation propagated through the sample beam ejected at a pressure of ~500-1000 mTorr from an effusive nozzle that was housed in the reaction chamber. The Ar (or O_2) gas was added to the chamber at a partial pressure controlled up to 3000 mTorr. The fragment emission signals were guided to the entrance of the FTIR spectrometer in which the movable mirror of interferometer was allowed to move step-by-step. The digitized signals, repeatedly collected for 30-100 laser shots, were monitored with an InSb detector cooled at 77 K and fed into a 200 kHz 16-bit transient digitizer for signal processing. The temporal resolution of IR signal was restricted at 5 μs with uncertainty of $<\pm(5x10^{-4})$%. The obtained interferograms were finally Fourier transformed to yield time-resolved spectra. The spectral responses of beamsplitter, optical filters, and detection system were all calibrated using an IR emitter serving as a blackbody-like radiation.

3. Results and Discussion

3.1. Photodissociation of CH_3COCl

As one of the simplest acyl halide compounds, acetyl chloride has been used as a prototype for the photochemistry studies.[6-8, 23-27] Its first UV absorption band from 210 to 280 nm peaking at about 240 nm was characterized by the

n(O)→π^*(C=O) transition.[7] Upon the $^1(n, \pi^*)_{CO}$ excitation at 248 nm, Butler and coworkers observed the release of highly anisotropic angular distributions of Cl atoms in a molecular beam experiment at cold temperature.[28-30] A fraction of the resultant CH_3CO fragment could further decompose to the ground state CO (v=0) with rotational levels up to J=30.[31] However, Kong and coworkers obtained the IR emission band of CO (v≤ 8) with temperature of 6900 K,[32] by applying higher laser fluence at 248 or 266 nm undergoing multiphoton absorption. Rowland and Hess obtained exclusively the HCl-ketene complex with a T-shaped structure in the Ar matrix-isolated photodissociation.[27] The HCl in the complex was generated from the hot ground state acetyl chloride via internal conversion.

Different from the above-mentioned dissociation channels, we have explored a new channel leading to HCl, CO, and CH_2 elimination in a one-photon dissociation of gas-phase CH_3COCl at 248 nm in the presence of Ar or O_2 gases using time-resolved FTIR emission spectroscopy.[33] The addition of Ar or O_2 helps regulate the relative yields of these fragments. As shown in Fig.1, a series of Ar pressure dependence of emission spectra of CO and HCl were obtained in the range of 1950-2250 and 2400-3200 cm^{-1}, respectively. Both CO and HCl fragments are hardly recognized until the Ar pressure is increased to 250 and 505 mTorr, respectively. The rotational population distribution of HCl with assignable spectra up to v=2 is characterized by a single-profile Boltzmann law. The temperature evolution of the HCl curves can be extrapolated to the zero delay time yielding 1140±90 and 760±50 K for v=1 and 2, respectively, and the subsequent total rotational energy of 1.4±0.2 kcal/mol. While assuming a Boltzmann-type distribution, vibrational temperature extrapolated to the zero delay time may be evaluated analogously to be 4700±300 K; the subsequent

vibrational energy becomes 7.5±1.1 kcal/mol by taking into account the contribution of v=0 and zero-point energy.

Like the case of photodissociation in the matrix isolation,[27] HCl is a primary dissociation product. However, an alternative channel to the HCl formation may result from the hot Cl atom in collisions with the parent molecule. The rate constant for such a reaction scheme,

$$Cl + CH_3COCl \rightarrow HCl + \text{other products,} \qquad (3)$$

was reported to be < $1x10^{-14}$ cm^3/molecule.s.[34] To confirm the possibility of eq.3, a straightforward experiment was carried out by adding Br_2 as a scavenger in the system. The reaction scheme of

$$Br_2 + Cl \rightarrow Br + BrCl \qquad (4)$$

has a rate constant of $3.62x10^{-10}$ cm^3/molecule.s at room temperature.[35] If any HCl fragment is contributed from the hot Cl reaction, its product yield should have been effectively suppressed by the Br_2 addition. The spectral intensities of HCl produced in the presence/absence of 200 mTorr Br_2 are found to be comparable, thereby suggesting that the secondary reaction channel should be neglected.[33]

As with the HCl analysis, the rotational population distributions of CO up to v=4 may be fitted with a Boltzmann distribution at temperature of about 300 K. The total rotational energy amounts to 0.57±0.09 kcal/mol, as averaged from the individual rotation energy of 0.6, 0.59, 0.57, and 0.47 kcal/mol for v=1, 2, 3, and 4, respectively, at 5 μs delay. The vibrational temperature extrapolated to the zero time delay is estimated to be 3190±60 K and the vibrational energy is obtained to be 5.7±0.9 kcal/mol. The CO fragment may not be contributed by the secondary dissociation of CH_3CO that yielded the CO product in the ground vibrational

state.[31] It is generated from one-photon dissociation, also different from those obtained by Li *et al.*[32]

When O_2 is adopted to replace the Ar colliders in the chamber, the enhancement of the fragment yields is as large as in the presence of Ar. If the fragments are dissociated from a triplet state of CH_3COCl, the addition of O_2 as an efficient triplet quencher should significantly suppress the product yields. The dissociation channel via ISC is excluded. The CO_2 product appears at 2250 cm^{-1} when O_2 is added, whereas it disappears when Ar is substituted. The reaction scheme,

$$CH_2(\tilde{X}\,^3B_1) + O_2 \rightarrow CO_2 + H_2, \qquad (5)$$

has a rate constant of 2×10^{-12} cm^3/molecule.s at 298 K.[36,37] As shown in Fig.2, a time-dependence of production yield of CO_2 can be fitted to yield a production rate constant of $(2.1\pm0.2)\times10^{-12}$ cm^3/molecule.s.[33] The agreement with that in the literature evidences existence of the CH_2 moiety.[36,37] However, we cannot distinguish which state is generated between $CH_2(\tilde{X}\,^3B_1)$ and $CH_2(\tilde{a}\,^1A_1)$, because their production rate constants of CO_2 are the same.[38]

As calculated in Fig.3, the ground state CH_3COCl dissociates to the products of CH_2=CO and HCl, the major pathway for HCl, by surpassing a barrier of 45.3 kcal/mol with a rate constant k_1 of 7.59×10^{11} s^{-1}, at least two orders of magnitude larger than the other pathways such as three-body concerted dissociation (CH_2 + HCl + CO) with k_7 of 3.87×10^{9} s^{-1} and two-body dissociation (CH_3Cl + CO) with k_2 of 7.79×10^{8} s^{-1}, followed by further dissociation to CH_2 + HCl that is kinetically disfavored. The HCl fragment may be alternatively produced through an isomerization intermediate (i1) of $CH_2C(OH)Cl$. While inspecting the related rate constants, k_5, k_{-5} and k_6

evaluated to be 9.70×10^{8}, 1.6×10^{9} and 5.52×10^{10} s^{-1} along the path, respectively, the reaction scheme $CH_3COCl \rightarrow i1 \rightarrow CH_2CO + HCl$ is restricted to a slow isomerization step and thus cannot contribute significantly. From the energetic aspect, it is probable for CH_2=CO to proceed a secondary dissociation to obtain the ground states CH_2 and CO. The resulting CO must be in the vibrational ground state, because the available energy is just slightly above the threshold energy for the C=C bond rupture. Therefore, the vibrationally excited CO fragment obtained above is expected to originate from the dissociation channel CH_3Cl + CO via a transition state of 86.8 kcal/mol.

Different from the dissociation channels reported previously, we find a new dissociation channel initiated on the ground state surface. The colliders added may regulate the IC efficiency, leading to enhancement of the fragment yields. The plausible mechanisms are interpreted from the energetic and kinetic points of view.

3.2. Photodissociation of CH_3COCN

The absorption spectra of gaseous acetyl cyanide in the range of 150 - 400 nm show a weak band at 300 nm attributed to the S_1(A"), $^1(n_O, \pi^*_{CO})$ state, while the onset of the second weak band near 230 nm and the successive strong band <200 nm are due to the S_2(A"), $^1(\pi_{CN}, \pi^*_{CO})$ and S_3(A'), $^1(\pi_{CO\text{-}CN}, \pi^*_{CO})$ transition, respectively.[12-14] Horwitz *et al.*[10] presented the first report on photodissociation of acetyl cyanide at 193 nm exciting the molecule to the S_3 state. They then probed the energy distribution of the primary CN(X) fragment using laser-induced fluorescence (LIF). At the same photolysis wavelength, North *et al.*[11] obtained the energy and anisotropic distributions of CN(X) using both high-resolution

transient frequency modulation spectroscopy and photofragment translational spectroscopy (PTS). Their results evidenced that the CN elimination is preferred to the CH_3 elimination. Furlan *et al.*[13] obtained a branching ratio of CN/CH_3 to be 85/15% by using PTS technique. Cheng group[14] proposed a dissociation mechanism to interpret why the CN(X) fragment is preferred. Owrutsky and Baronavski[12] determined the unimolecular decomposition rates at 193 nm using femtosecond mass-resolved photoionization spectroscopy.

The S_3(A') state of acetyl cyanide has strong diabatic coupling directly with the $^1(n_N, \sigma_{C-CN}^*)$ repulsive configuration or S_3(A') may cascade through S_2(A") prior to the coupling, thereby yielding the predominant CN fragment.[14] In contrast, the S_1(A"), $^1(n_O, \pi^*_{CO})$ band origin is at 363.5 nm and extended to ~230 nm.[15] Its fluorescence lifetime varies from 0.53± 0.02 μs[39] to 3.5± 0.3,[15] as excited from 292.0 to 363.5 nm. The S_1(A") state should have a weak coupling strength with its neighboring $^1(n_N, \sigma_{C-CN}^*)$ state such that its lifetime is longer. In this manner, the photofragments may be readily initiated through the S_1 - S_o coupling.

Thus far, photodissociation starting from the S_1 or energetic S_o has been seldom studied except for some theoretical predictions.[40-42] To prepare the acetyl cyanide populated in the S_1 state, we selected the photolysis wavelength at 308 nm.[16] An effusive beam of CH_3COCN was irradiated in the presence of Ar gas at 2000 mTorr. The dissociation fragments were then detected using time-resolved FTIR emission spectroscopy. Fig.4a shows delay-time dependence of the HCN emission spectra at a resolution of 0.5 cm^{-1} ranging from 3100 to 3400 cm^{-1}. The rotational state distribution evolves to two narrow components for the P and R branches with the maximum intensities at 9 μs delay. Fig.4b shows the ν_3 spectrum of H-CN stretch mode that is assigned up to (v, J)=(2, 24) with a

signal-to-noise ratio larger than 2. The corresponding rotational energies E_{rot} are then evaluated to be 2.87±0.05 and 0.91±0.05 kcal/mol for the HCN v=1 and 2, respectively, and the total rotational energy amounts to 2.11±0.05 kcal/mol. Given the HCN (v=1 and 2) population, the Boltzmann vibrational temperature is approximately estimated and the subsequent vibrational energy is estimated to be 17±2 kcal/mol by taking into account the contribution of v=0 and zero point energy.[16]

Fig.4a also shows the delay-time dependence of CO emission spectra from 1900 to 2200 cm^{-1}. Given a Boltzmann law, the rotational population distributions of CO, assignable up to J=27, 25, and 20 for v=1, 2, and 3, respectively, yield the corresponding rotational temperature of 520±30, 410±20, and 400±40 K and the rotational energy of 0.86±0.07, 0.84±0.02, and 0.79±0.02 kcal/mol. Thus, the average rotational energy amounts to 0.84±0.02 kcal/mol. Given the vibrational population for each state, the vibrational energy is estimated to be 6.7±0.7 kcal/mol.[16]

To interpret how the CO fragment is eliminated, we found a pathway leading to the CO + CH_3NC products via isomerization TS at 94±2 kcal/mol.(Fig.5a)[43] A prior distribution method[44-46] was further conducted to characterize the vibrational energy distribution of CO on a statistical basis. Based on the energy level scheme in Fig.5a, the densities of product states were calculated by direct counting with a discretization energy of 10 cm^{-1}. For performing the prior distribution calculations, the asymptotic energy at 84.0 kcal/mol of radical channel, $CH_3C(O)CN \rightarrow CH_3$+NCCO, was assumed to be the extreme limit of triple fragmentation ($CH_2(\tilde{a}^1A_1)$+CO+HCN). Fig.5b shows the results along with the experimental findings (CO(v=1~3)). The pathway to

CH_3NC + CO yielded a vibrational branching ratio (v=0:1:2:3~0.63:0.25:0.093:0.032) in excellent agreement with the observation (0.62:0.25:0.09:0.05). The vibrational energy disposal of CO can be appropriately predicted based on the statistical method. Accordingly, the CO fragment is verified to stem from a primary pathway to CO + CH_3NC. The CO contribution from a three-body breakup (CO + CH_2 + HCN) is negligible, because the vibrational branching ratio along this channel is v=0:1:2~ 0.993:0.07:0:0.

To inspect the possibility of the CH_2CO moiety undergoing a secondary dissociation, O_2 is added to react with the resultant CH_2. A weak CO_2 spectrum does appear at 2250 cm^{-1}, evidencing the CH_2 existence. But the CO fragment is substantially dissociated from the primary channel CO + CH_3NC.

In the calculations of reaction pathways,[16] HCN may be eliminated on the ground state surface of CH_3COCN by surpassing a transition state (ts_{HCN}) at 67.8 kcal/mol with a reaction rate constant of $6.16x10^8$ s^{-1}. The reaction scheme $CH_3COCN \rightarrow CH_2CO$ + HCN is endothermic by 21.8 kcal/mol, in contrast to the one $CH_3COCN \rightarrow CH_3CO$ + CN with endothermic energy of 100.7 kcal/mol that cannot be overcome at 308 nm, equivalent to the photolysis energy of 92.8 kcal/mol.[16] The ts_{HCN} structure shows a H-CN distance of 1.821 Å, much larger than the bond length 1.066 Å in the HCN product. That is why HCN is dissociated with v_3 stretch mode vibrationally hot. Similarly, HNC can be eliminated on the ground state CH_3COCN via ts_{HNC} at 63.8 kcal/mol with a rate constant calculated to be $1.44x10^9$ s^{-1}. However, as shown in Fig.4b, less emission intensities from H-NC v_1 stretch mode is obtained in the range of 3450-3750 cm^{-1}.[16] Only a few rotational lines can be assigned, as restricted to a poor signal-to-noise ratio. While inspecting the ts_{HNC} structure, HNC is found to have a bending angle of 122.8° and a H-NC bond distance of 1.651 Å. The fragmented

HNC is expected to substantially populate in the bending mode at 464 cm^{-1}, which is beyond the spectral range detected. The v_1 stretch mode must be less populated such that the emission intensity is weak. We fail to find any CH_3 and CN fragments in the spectral region of 2950-3450 cm^{-1}(ref.47) and 1912-2131 cm^{-1},(ref.48) respectively, which dominate the dissociation products at 193 nm.

Upon irradiation at 308 nm, the HCN and HNC fragments are anticipated to eliminate from CH_3COCN on the singlet ground state surface by the collision-induced IC. The dissociation channel via ISC is excluded by examination with O_2. The collision-induced rate constant may be determined by the following processes. As shown in Fig.6, the HCN intensity, obtained by the area integration over the corresponding low-resolution spectra, increases proportionally to the Ar pressure. The kinetic behavior caused by the Ar collision-induced IC can be characterized as follows:[16]

$$[S_0] \xrightarrow{h\nu\ 308\text{nm}} [S_1] \begin{cases} \xrightarrow{k_{rad}} [S_0'] + h\nu \\ \xrightarrow{k_{\text{int}}} [S_0]^* \xrightarrow{k_{RRKM}} [HCN] \end{cases} \qquad (6)$$

The coupled differential rate equations comprising $d[S_1(t)]/dt$, $d[S_o'(t)]/dt$, and $d[S_o^*(t)]/dt$ may be solved exactly. Here, k_{int} is further divided into two terms,

$$k_{\text{int}} = k_{\text{int}}^{S}[S_0] + k_{\text{int}}^{Ar}[Ar] \qquad (7)$$

The first IC term is caused by the precursor, while the second term is attributed to the collisions by Ar. Given k_{RRKM} calculated to be 6.2×10^{8} s^{-1} and k_{rad} measured to be 2.2×10^{6} s^{-1},[16] the Ar dependence measurements can be fitted appropriately and the k_{int}^{s} and k_{int}^{Ar} are then optimized to be 1.5×10^{-12} and 1.0×10^{-12} $cm^3molecule^{-1}s^{-1}$, respectively. When the rate constants are increased to 1×10^{-11} $cm^3molecule^{-1}s^{-1}$, the fitting curve deviates significantly from the experimental findings.(Fig.6)

The molecular fragments of HCN, HNC, CO, and CH_2 are produced from CH_3COCN on the S_o ground state surface via the S_1-S_o coupling. The Ar collisions facilitate the IC process and enhance the product yields. Different from the photodissociation phenomena initiated from the S_3 state, the major CN and CH_3 fragments are generated by diabatic coupling with the $^1(n_N, \sigma_{C-CN}^*)$ state. This example shows that the nonadiabatic product channel may be regulated through the tuning of photolysis wavelength.

3.3. Photodissociation of CH_3COSH

As one of asymmetrically substituted carbonyl compounds, the ground state structure of thioacetic acid (CH_3COSH) has been well characterized, but its photochemical behavior has received much less attention. Nagata *et al.*[49] probed the electronic spectra of CH_3COSH in cyclohexane (ethanol) solution and assigned the shoulder and peak transitions to the (n_O,π^*_{CO}) and (π_S,π^*_{CO}) bands occurring at 268 (266) and 219 (221) nm, respectively. To the best of our knowledge, Romano *et al.*[50] reported the first example of CH_3COSH photochemistry in a study of matrix isolation. The CH_3COSH isolated in solid Ar at 15 K was irradiated with broad-band UV-visible light ($200 \leq \lambda \leq 800$ nm), yielding the following three dissociation pathways,[50]

$$CH_3COSH \rightarrow CH_2CO + H_2S \quad (8)$$

$$\rightarrow OCS + CH_4 \quad (9)$$

$$\rightarrow CO + CH_3SH \quad (10)$$

in which the reaction (8) is predominant. From the theoretical point of view, Lu *et al.*[51] calculated the thiol form ($CH_3C(O)SH$) to be more stable by 4.3-5.9 kcal/mol than the thione form ($CH_3C(S)OH$) with a tautomerization barrier of

28.6-30.2 kcal/mol. Thus, decomposition of the ground state thioacetic acid is dominated by the thiol form.

The UV/Vis absorption measurement of gaseous CH_3COSH from 200 to 600 nm shows a rise at 250 nm with two peaks at 215 and <200 nm.[22] As referred to the absorption spectrum in the solution,[49] the former absorption is ascribed to the (n_O,π^*_{CO}; S_1) band, while the latter is ascribed to the (π_S,π^*_{CO}; S_2) band. CH_3COSH may thus be excited to the (n_O,π^*_{CO}; S_1) state using the wavelength at 248 nm with an absorption cross section determined to be $(8.84\pm0.13)\times10^{-20}$ cm^2.[22] The corresponding radiative lifetime and self-quenching rate constant were also determined to be 249±11 ns and $(4.13\pm0.07)\times10^{-10}$ $cm^3molecule^{-1}s^{-1}$ by using LIF technique.[22] The self-quenching rate is contributed by the processes of the $S_1 \rightarrow S_0$ collision deactivation, internal conversion or intersystem crossing.

Thus far, the photochemical behavior of gaseous CH_3COSH has never been characterized before. As with the case of CH_3COCN, if the photolysis wavelength at 193 nm is selected, then the S_2 state promotion will lead to elimination of SH (or OH depending on which isomer is excited) and CH_3 by diabatic coupling with the adjacent C-S (or C-O) and C-C bonds as predicted by the Norrish type I reactions. Instead, we select the photolysis wavelength at 248 nm to prepare the gaseous CH_3COSH in the S_1 state with a longer lifetime. We then expect a distinct photodissociation mechanism should occur by opening up different nonadiabatic dissociation pathways.

An effusive beam of CH_3COSH at a pressure of 1500 mTorr was irradiated at 248 nm in the presence of Ar gas at 3000 mTorr.[22] The dissociation fragments were then detected. The 5 μs-resolved FTIR emission spectra of CO fragment were found to be resolved with the rotational lines up to J=40, 36, and 30 for v=1, 2, and 3, respectively. Given the Einstein spontaneous emission coefficients, each

rotational population distribution of CO (v=1, 2, and 3) was well characterized by a Boltzmann law. The Boltzmann rotational temperature was then determined to be 1429±42, 1290±53, and 1126±71 K for CO v=1, 2, and 3, respectively. The corresponding rotational energies are evaluated to be 2.21±0.04, 1.85±0.01, and 1.51±0.01 kcal/mol, thus amounting to 2.0±0.2 kcal/mol for an average rotational energy. Given the vibrational population for each state at 0 μs delay, the Boltzmann vibrational temperature is 3446±340 K and the vibrational energy yields 6.7±0.7 kcal/mol.

While closely examining the CO spectral baseline, there exists a broad unresolved profile extending from 1950 to 2150 cm^{-1} that is expected to come from the OCS fragment. This product has three modes of the CS stretching v_1, bending v_2, and CO stretching v_3 peaking at 849.8, 520.7, and 2070.9 cm^{-1} with the A-coefficient of ~0.097, ~0.042, and ~2.67 s^{-1}, respectively.[52] Thus, only the v_3 mode with a rotational constant of 0.2029 cm^{-1} may be observed by the InSb detector, but cannot be resolved with a 0.25 cm^{-1} resolution. After enlarging the OCS profile as a function of the delay time, Fig.7 shows that OCS can be excited up to v=6 at 1957 cm^{-1} at 10 μs delay, prior to relaxing toward low v and then vanishing after 280 μs delay. On the other hand, the CH_2CO spectra with vibrational mode v_2 at 2150 cm^{-1} overlap with the OCS spectra and might contribute to the region of 2100-2200 cm^{-1}.[53] As with OCS, its spectral intensity decreases with the delay time.

As shown in Fig.8, the spectral region comprises three profiles at about 2590, 2920, and 3000 cm^{-1}. We expect CH_3SH dominates the first two regions,[54] while CH_4 dominates the third one.[55] Since the A-coefficient of H_2S fragment is comparable to that of CH_3SH v_3 mode, we thus expect H_2S should partially contribute to the 2590 cm^{-1} region. Despite a poor signal-to-noise ratio in

characterizing the products CH_4, H_2S, and CH_3SH, their accompanying moieties OCS, CH_2CO, and CO have been identified above. Thus, with the aid of theoretical calculations,[51] three dissociation channels may be verified leading to the products of CH_3SH + CO, CH_2CO + H_2S, and CH_4 + OCS. A fraction of the product CH_2CO was found to decompose to CH_2 and CO. The CH_2 fragment was verified by examination with O_2.

According to the calculations of dissociation pathways shown in Fig.9a, CH_3COSH syn-I structure is dissociated on the ground state surface via a TS at 55.5-57.2 kcal/mol to the products CH_2CO + H_2S, or via a TS at 90.8-91.5 kcal/mol to CH_3SH + CO.[51] The syn-I compound may undergo isomerization to anti-I form, followed by decomposition to CH_4+OCS via a TS at 66.8-67.9 kcal/mol. The dissociation channel to CH_2CO + H_2S is dynamically most favorable, since its TS barrier is smaller. The dissociation may alternatively proceed from the other thione tautomer, yielding CH_2CS + H_2O, CH_3OH + CS, and CH_4 +OCS.[51] However, such tautomer dissociation is slowed by a tautomerization barrier, as compared with the thiol form. The products of CH_2CS, H_2O and CS were not found by the FTIR emission spectroscopy.

Like the behavior of Norrish type I reaction, the (n_O,π^*_{CO}; S_1) band excited at 248 nm may couple to the adjacent single bonds yielding the radicals of CH_3 or SH. These radicals could recombine in a favorable orientation to yield the products observed. If the product formation involves the radicals such as CH_3 that must be dissociated from a triplet state, the addition of O_2 should significantly suppress the product yields. Thus, the CH_3SH formation through the radical recombination is neglected.

To further identify which pathway between primary and secondary decomposition leading to the CO production, the prior distribution method is

again adopted for analysis.[44-46] As show in Fig.9b, the prior distributions of CO vibrational energy are evaluated along with the experimental results. The vibrational state of CO produced in three-body breakup ($CO+CH_2+H_2S$) reaches only to v=1. However, the CO along the CH_3SH + CO pathway yields a vibrational branching ratio (v=1:2:3~1:0.49:0.23) in appreciable agreement with the experimental findings (1:0.40:0.17). The product CO is evidenced via the primary channel of CH_3SH + CO.

As compared to the gas-phase dissociation, CH_3COSH in the matrix-isolated experiment[50] leads to the same three dissociation channels. Both dissociation mechanisms are initiated on the ground state surface. In the FTIR method the Ar addition facilitates the IC process. All the product signals are enhanced to the same extent and thus their branching ratios remain the same, independent of the Ar pressure. In contrast, a broad-band UV-visible light source adopted in the matrix photochemical study covers simultaneously two excitation bands, (n_O,π^*_{CO}) and (π_S,π^*_{CO}), making the dissociation pathways complicated. Further, the matrix cage effect often brings about new species generation that cannot be formed under the regular gas-phase condition.

3.4. Photodissociation of CH_3CHO

While investigating the molecular channel CO + H_2 dissociated from formaldehyde (H_2CO) early in 1990's, Moore and co-workers found appearance of an abnormal CO rotational distribution that cannot be explained by conventional transition state (TS) mechanism.[56] This phenomenon was later thoroughly characterized as an alternative mechanism so-called "roaming" atom or radical by Suits and Bowman and their co-workers about a decade ago.[57,58]

Since then, molecular photodissociation dynamics was widely explored to look into such a roaming signature.[59] For instance, when acetaldehyde (CH_3CHO) is irradiated with UV light, the molecules may release the ($CO + CH_4$) products on the ground state surface S_o via a tight TS. In addition, an alternative roaming pathway is found to initiate from the barrierless radical products ($HCO + CH_3$) on the ground state surface.[59-63] Then, the incipient radicals meander with slow motion around varied configuration spaces in the weak attractive field of the moieties and ultimately undergo intramolecular abstraction to form the same molecular products.

In a study on photodissociation of CH_3CHO at 308 nm, Houston and Kable have obtained a bimodal rotational distribution of CO at v=1 using LIF technique;[61] the low-J component was anticipated to result from a CH_3-roaming pathway, while the high-J component was ascribed to the conventional TS contribution. They then determined the branching ratios of CH_3-roaming/TS mechanism to be 13/87% at CO v=1 and 0/100% at v=2. Kable and coworkers recently reassigned the low-J, slow speed component of CO fragment to the H-roaming by probing CO with (2+1) REMPI ion-imaging in the wavelength range of 308-328 nm.[59] When detuning the wavelength between 325 and 328 nm, they found this component disappears, because the photolysis energy becomes lower than the bond-breaking threshold of $H + CH_3CO$. As referred to the quasi-classical trajectory (QCT) results,[60,64] the high-J component of the CO distribution was reassigned to the CH_3-roaming. The branching fractions of CH_3-roaming, H-roaming and TS pathway were then evaluated to be 71±12%, 13±3% and 16±10%, respectively, in photolysis at 308 nm.[59] Among them, the TS contribution is estimated from the QCT result,[60] but has not been observed experimentally. In fact, when the QCT calculations were initiated at the

conventional saddle point (SP), a low energy component <75 kcal/mol, peaking at ~30 kcal/mol (see Fig.11), appeared in the CH_4 vibrational population, but it was not found in the experiments.[60] For this reason, we approach differently using time-resolved FTIR emission spectroscopy.[65]

As acetaldehyde is promoted to the (n_O,π^*_{CO}; S_1) band by one-photon absorption at 308 nm, the acquired FTIR emission spectrum contains the CO fragment within 1900-2200 cm^{-1} and the CH_4, CH_3 and HCO fragments in the region of 2300-3300 cm^{-1}. When 600 mTorr CH_3CHO is irradiated in the presence of Ar at 3000 mTorr, a series of 5 μs-resolved CO spectra are well resolved. An example is given in Fig.10a, showing a comparison between CO spectrum acquired in 2 μs delay, with respect to the laser firing, and the simulated counterpart following photolysis at 308 nm.[22,65-67] The rotational spectrum for v=1 is fitted consistently with a bimodal Boltzmann population distribution, while the v=2-4 results can be fitted individually with a single Boltzmann population distribution. After extrapolating to the real zero time that is free from the Ar collisions, the bimodal feature is characterized by two Boltzmann rotational temperatures of 1150±80 and 200±20 K for CO v=1; a single Boltzmann rotational temperature is obtained to be 950±70, 790±70, and 680±60 K for the v=2, 3 and 4, respectively. The CO rotational and vibrational energy disposal are then evaluated to be 1.9±0.1 and 7.2±0.7 kcal/mol, respectively.[22,66,67] As shown in Fig.10b, the bimodal distribution can break into two Boltzmann rotational components during the μs period of instrument response. The ratio of low-/high-J component at the zero delay time is evaluated to be (10±2)/(90±5)% at v=1, consistent with the value of 13/87% by the LIF method.[61] Such consistency is indicative of reliability of the branching evaluation without suffering from the collision interference.

The accompanying CH_4 product acquired in the spectral region of 2500-3100 cm^{-1} is solely due to Δv_3= -1 C-H stretching emission. The CH_4 spectrum is complicated by concomitant appearance of rotational spectrum and also interfered by a small profile of the H-CO stretch mode v_1 at 2434.5 cm^{-1} and the CH_3 antisymmetric stretch v_3 at 3150 cm^{-1}.[68] The CH_3 and HCO emission signals almost vanish in 5-10 μs delay. The CH_4 spectrum was thus acquired in 7 μs delay to minimize the spectral overlap with HCO and CH_3. According to the method reported previously,[60,67] the CH_4 vibrational distribution can be separated from the rotational contribution. Given the factor of harmonic line intensity, the pure vibrational spectrum of CH_4 is extracted by deconvolution from its rotational distribution assumed at 500 K and the instrument resolution function (15 cm^{-1}), and then the subsequent vibrational energy distribution is determined with the aid of the maximum entropy model (Fig.11a).

A bimodal vibrational distribution of CH_4 is thus obtained; the high-energy component is consistent with the results by Heazlewood *et al.* (Fig.11b),[60] while the low-energy component peaking at ~25 kcal/mol may be fitted with a Gaussian distribution (Fig.11a), consistent with the QCT prediction for the TS pathway.[60] The low-/high-energy component yields a ratio of (25±5)/(75±13)%. As compared with the low-energy component observed, the theoretical counterpart is also characterized by a Gaussian distribution, but shifts to a higher energy region by about 10 kcal/mol.[60] It may rise from a larger available energy adopted in the calculations, containing both photon energy equivalent to 308 nm and zero-point energy. As for the high-energy component, the CH_4 product is anticipated to result from both H- and CH_3-roaming pathways.[59]

Fig.12 displays the energy states for three pathways,[59,60] in which the conventional SP lies at the same state as the CH_3-roaming SP, and the H-roaming

SP, unfounded yet, is expected to be close to the energy state of the related molecular products. Then, the available energy via the H-roaming mechanism is allowed for population up to CO v=1 state, but cannot reach those states higher than v=1. That is why the H-roaming signature is found only in the low-J distribution of CO(v=1), but disappears in CO(v≥2) in which the remaining single-modal distribution is attributed to the CH_3-roaming mechanism. Given the CH_4 vibrational and CO(v=1) rotational bimodality, the branching fractions of H-roaming, CH_3-roaming and TS contribution are evaluated to be (8±3)%, (68±10)%, and (25±5)%, respectively, in consistency with those reported by Kable and coworkers,[59] while considering the uncertainty.

The new assignment reported[59] has been confirmed by the FTIR method,[65] but the signature of TS pathway is found for the first time in the CH_4 moiety. A single-modality of CH_4 vibrational distribution was observed earlier using similar time-resolved FTIR emission spectroscopy (Fig.11b).[60] The discrepancy of the CH_4 distribution arises from different experimental conditions. The enhancement of the collision-induced IC facilitates the dissociation channels via highly vibrational states of the ground potential energy surface and thus increases the reaction rates through the TS pathway.

3.5. Photodissociation of $HCOOCH_3$

As a syngas precursor, photodissociation of methyl formate ($HCOOCH_3$) follows a distinct mechanism different from the thermal decomposition through which high-purity CO can be generated.[69,70] By using photofragment translational spectroscopy (PTS), Lee[71] reported four primary dissociation pathways for methyl formate-d ($DCOOCH_3$) at 193.3 nm, including the channels

of $CH_3O(\tilde{X}^2E)$+DCO($\tilde{X}^2A'$), $CH_3O(\tilde{X}^2E)$+DCO($\tilde{A}^2A''$), $CH_3OCO(\tilde{X}^2A')$+D(^2S), and $CH_3OD(\tilde{X}^1A')$ + CO($X^1\Sigma^+$). The atomic and radical fragments detected above were not found in the thermal decomposition. Further, the molecular formation of CH_3OH + CO is a minor channel, but it is regarded as the major one in the pyrolytic process.

Chao *et al.*[72] focused on the molecular channel of CH_3OH + CO(v=0) in the photodissociation of $HCOOCH_3$ at 234 nm using velocity ion imaging coupled with (2+1) REMPI technique. Later, Tsai *et al.*[73] extended the photolysis wavelength from 225 to 255 nm. They acquired the ion images of CO(v=0) at different rotational levels J to look into the corresponding translational energy distribution. As CO rotational levels (J_{CO}) are large, only a broad component with a large average translational energy appears. As J_{CO} decreases, a bimodal energy distribution arises comprising a sharp component and the above-mentioned broad component. The large broad translational component is ascribed to the conventional TS pathway, while the small sharp component is ascribed to a roaming mechanism, which is characterized by a low rotational energy deposition in CO in conjunction with a small total translational energy release. The branching ratio of roaming pathway increases with decreasing J_{CO}.

From a theoretical point of view, they further constructed a reduced-dimensional PES of ground state $HCOOCH_3$ in which the OCH_3 group is frozen as a unit. Fig.13 shows the configurations and energies of conventional TS and conical intersection, reported by Cui *et al.*,[74] between the excited and the ground state surfaces. Based on the ground state PES, the QCT calculations were performed with initial configurations near the conical intersection to obtain the CO kinetic energy distributions for triple fragmentation ($H+CO+CH_3O$) and molecular production. When the photolysis wavelength is

shorter than 248 nm, the HCO radical gains enough energy to break the H—CO bond.[73] In the molecular channel, the roaming CO can be produced by molecular wandering along the radical channel prior to falling down in the molecular exit valley. Alternatively, the energetic population in S_o may surpass the tight TS to form the same molecular products. The consistency between experimental findings and QCT results is conducive to gaining insight into the role of roaming pathway played in production dynamics of CO fragments.[73]

Recently, the CO (v=1) ion images were probed at the selected rotational levels of J = 2, 7, and 11 in photodissociation of methyl formate at 248 nm.[75] This photolysis wavelength fails to proceed the triple fragmentation ($H+CO(v=1)+CH_3O$). As shown in Fig.14, the CO images show an isotropic angular distribution and a bimodal translational energy distribution in the center-of-mass frame for each J level selected. Note that the images at higher J and v could not be acquired because of the poor signal-to-noise ratio. Two translational energy profiles were then resolved by using Boltzmann-like functions. These data were compared with those obtained by QCT simulations.[75] The sharp cold component peaking at 2 kcal/mol is attributed to the roaming process, while the broad component peaking at 5–6 kcal/mol is ascribed to the conventional TS mechanism (Fig.14). The normalized yields of the two mechanisms were evaluated by means of the integrated area of the deconvoluted profiles. The roaming fraction yields 0.29 ±0.07, 0.20±0.09, and 0.17±0.04 for J = 2, 7, and 11, respectively, corresponding to an average of 0.2±0.1, while the fraction along the TS path is 0.71± 0.12, 0.80 ± 0.20 and 0.83 ± 0.08. The roaming fraction tends to decrease as J increases. Under the assumption of a Boltzmann distribution, the rotational temperatures of the CO products may be estimated to be 200 K for roaming and 420 K for the tight TS channel.

To compare with the CO (v=1) results obtained by ion imaging, we acquired the rovibrational energy deposition in CO (v≥1) following photodissociation at 248 nm using time-resolved FTIR emission spectroscopy. The CO vibrational spectra from v=1 to 4 has been assigned clearly, but the populations of higher vibrational states are small and are neglected. Among them, the bimodal rotational distributions for v = 1 and 2 are obtained, as shown in Fig.15. The energy disposal in vibrational and rotational degrees of freedom could then be analyzed. The FTIR measurement of CO (v=1) gave a rotational temperature of 470 and 1080 K for the roaming and the tight TS, respectively, and a roaming fraction of 0.3±0.04 consistent with the roaming results by the ion imaging. The discrepancy of the rotational temperatures could be due to difference in the experimental conditions. The parent molecules are cooled down in the molecular beam experiment, while the FTIR measurements are performed at room temperature in the presence of Ar colliders. The collision-induced IC should enhance the rovibrational population of parent molecules prior to decomposition and subsequently yield a hotter rotational and vibrational energy disposal.

In the FTIR experiment with the Ar addition, the IC and ISC processes are enhanced to allow for a detailed analysis of CO spectra with a better signal-to-noise ratio, despite suffering from small Einstein emission coefficients in the IR region. Accordingly, the method obtained the full rotational bands for v = 1-4 and even higher, and rotational bimodality for v = 1 and 2. In contrast, the beam experiment with ion-imaging obtained the vibrational population only at v=1 with a few of low rotational levels.

3.6. Summarized Highlights

Among the five carbonyl compounds with non-Norrish type I reaction, the photodissociation process is initiated from the same $^1(n, \pi^*)_{CO}$ lower state, which can be promoted by either 248 or 308 nm, depending on a shift of the corresponding absorption spectrum by the electron donating or withdrawing character of the functional groups attached to CO. The lowest excited state is thus selected to avoid electronic state-coupling complication rising from the higher states.

The nonadiabatic dissociation process essentially relies on the diabatic coupling strength with the neighboring $^1(n, \sigma^*)$ state. If the coupling strength is strong, then the adjacent single bond fission may probably take place. Photodissociation of CH_3COCl belongs to this case. The strong strength of state-to-state coupling causes rapid elimination of the Cl (or Cl*) atoms from a repulsive $^1(n, \sigma^*)$ state and thus shortens the excited-state lifetime within the picosecond range. In contrast, when the coupling strength is weak, the excited state prepared has a longer lifetime such that the nonadiabatic dissociation may rise preferentially from the ground state via IC or the triplet state via ISC. The compounds, CH_3COCN and CH_3COSH, belong to this case.

The method with addition of the Ar (or O_2) gas in the reaction chamber is adopted herein to regulate above-mentioned nonadiabatic dissociation processes. The efficiency of collision-induced IC or ISC is enhanced to compete for the excited-state population with the existing dissociation channels. However, it is somehow difficult to understand why a few Torr of Ar added may have chance to induce IC occurrence in the case of CH_3COCl. If all the CH_3COCl molecules dissociate as rapidly as within the picosecond regime, then the presence of Ar or O_2 does not have any chance to take part in the IC process. Such a short

photodissociation lifetime was measured under jet-cooled temperature of 10-30 K,[25] which allows for only a narrow population spread in the ground and excited state. As temperature is increased to ~300 K, the molecules are likely to populate in different vibrational levels and modes of the excited state, which may result in different molecular symmetric properties to dramatically change the dissociation efficiency.

An analogous example is given in the isomerization reaction of vinylidiene ($H_2C=C$)→ acetylene (HCCH). The lifetimes of vinylidiene were calculated to vary from 10^{-2} to 60 ps depending on the vibrational mode selected.[76,77] Levin *et al.*[78] studied unimolecular reaction of a highly excited vibrational state of acetylene using Coulomb explosion imaging technique. The vinylidiene isomer surprisingly survived for a period of at least 3.5 μs by measuring the density function of nuclear conformations. Therefore, when CH_3COCl is populated in some vibrational modes with slowed predissociation processes, the collision-induced IC is likely to yield new dissociation fragments such as HCl, CH_2, and CO. The opening of new channel resulting from a small amount of CH_3COCl population in some particular vibrational modes turns out to be a minor one, as compared to the major channel of Cl elimination.[33] A similar case is found in the photodissociation of C_2H_5COCl at 248 nm, as mentioned in Introduction Section,[18] giving rise to a minor dissociation channel initiated from the ground states.

In the photodissociation of CH_3COCN, when the excited state S_3, $^1(\pi_{CO\text{-}CN}, \pi^*_{CO})$ promoted at 193 nm is lowered to the S_1 state at 308 nm, the diabatic coupling strength with the $^1(n_N, \sigma^*_{C-CN})$ repulsive state becomes much weakened such that the CN and CH_3 elimination turns out to be kinetically and energetically disfavored. There is not any experiments carried out in a

supersonic jet, with which we expect it is not easy to find out all the fragments as reported with the FTIR method. In addition, the internal energy disposal obtained in each fragment will be different. To the best of our knowledge, no other competing channels occurring from the S_1, $^1(n_O, \pi^*_{CO})$ state of CH_3COCN have ever been found.

Despite the fact that the same fragments of $CH_2CO + H_2S$, $CH_3SH + CO$, and $CH_4 + OCS$ were reported under the matrix-isolation condition, it is hard to identify whether these fragments are all initiated from the ground state surface or in part produced by the matrix cage effect. For instance, Butler and Lee and co-workers[79] conducted photodissociation of gaseous acryloyl chloride (CH2CHC(O)Cl) at 193 nm, obtaining HCl four-center elimination from $CH_2ClCHCO$ isomer which is formed by 1,3-Cl shift of CH2CHC(O)Cl. Pietri *et al.* obtained similarly the $CH_2ClCHCO$ isomer in an Ar-matrix experiment.[80] However, it was suggested[79] that the $CH_2ClCHCO$ isomer may be formed with the aid of the matrix cage effect on which the Cl fragment released from C−Cl bond fission recombines with CH_2HCO. Further, the matrix experiment yields the fragments lying in the lowest rotational and vibrational states, but lacks the knowledge of the rovibrational spectra such as HCN and CO acquired herein.

CH_3CHO and $HCOOCH_3$ are classified to the same type of compounds. Their photodissociation results in molecular products of $CH_4 + CO$ and $CH_3OH + CO$, respectively, following both transition state and roaming pathways on the ground state surface. Note that this type does not exclude the possibility of the excited-state photodissociation. In fact, the excited states of both compounds readily decompose to the radical products including $HCO + CH_3$ and $HCO + CH_3O$. But we are concerned with the molecular products rising from the ground state surface.

Upon irradiation with the same photolysis wavelength, the molecular beam experiment and the current method both lead to the same molecular products through the S_1/S_o (or S_1/T_1) nonadiabatic processes, but the products generated in the FTIR experiment bear much larger internal energy. For instance, the prior studies on CH_3CHO performed at 308 nm under collision-free condition[60, 81-83] or with a low-pressure thermal cell[84] show that the S_1/S_o IC process is likely to play a minor role.[81,85] Most molecular products ($CO + CH_4$) on the S_o surface are expected to follow the ISC-based routes and the resulting CO is populated at lower vibrational states. However, the presence of Ar colliders in the FTIR experiment enhances the IC and ISC efficiency that ends up with two facts. First, the collision-induced S_1/S_o IC process renders a large available energy partitioned into CO that is vibrationally excited up to v=4. Second, the CH_4 + CO production is facilitated along the conventional TS pathway on the S_o surface, because deposition of the internal energy in the ground state CH_3CHO is large enough to surpass the transition-state barrier.

For the case of $HCOOCH_3$, the enhancement of IC and ISC processes increases the rotational and vibrational population of the fragments to much higher states, as compared with the molecular-beam results. The vibrational states up to v=4 are acquired with rotational levels larger than J=30 assignable. In fact, even higher vibrational states are detected, but neglected for poor signal-to-noise ratio. The roaming signature is found for the vibrational state at v=1 and 2. In contrast, the roaming pathway can be monitored only at v=1 for the beam experiment. Since the vibrational states are populated to v=4 and even higher, the roaming dynamics as a function of vibrational state may be studied in the future.

4. Conclusion

Some carbonyl compounds including CH_3COCl, CH_3COCN, CH_3COSH, CH_3COH, and $HCOOCH_3$ are UV-photolyzed in the presence of Ar gas in the reaction chamber and the corresponding fragments are detected using time-resolved FTIR emission spectroscopy. The enhancement of the collision-induced internal conversion or intersystem crossing facilitates the dissociation channels via highly vibrational states of the ground S_o or T_1 potential energy surfaces. In this manner, the corresponding products appear to differ distinctly from those especially in the supersonic jet experiments. If the diabatic coupling strength with the neighboring state is strong such as the case of CH_3COCl, the photodissociation is initiated from the excited states to cause the adjacent single bond rupture. The Cl (or Cl*) elimination dominates over the dissociation channels in a CH_3COCl molecular beam experiment at 248 nm. In contrast, the dissociation channels leading to the HCl, CO, and CH_2 fragments are open, as regulated by Ar collision-induced internal conversion.

Even if the dissociation process rises from the same ground state, the products obtained between supersonic jet and the current FTIR experiments are characterized with different energy disposal. For the case of acetyl cyanide, the primary products of HCN, HNC, and CO and a secondary product of CH_2 are obtained from the S_1 ($^1(n_O, \pi^*_{CO})$) dissociation at 308 nm through the S_1 - S_o coupling. Thus far, no molecular beam experiments have been found. CH_3COSH in the S_1 (n_O,π^*_{CO}) state excited at 248 nm yields three production channels of CH_3SH + CO, CH_2CO + H_2S, and CH_4 + OCS, which are essentially the same as those conducted under the matrix-isolated condition. In the latter experiment a

matrix cage effect often generates new species and the fragments are produced in the lowest ro-vibrational state.

The photodissociation of CHCHO and $HCOOCH_3$ leads to the molecular products CH_4 + CO and CH_3OH+CO, respectively, on the ground state surface through both transition state and roaming pathways. Following photodissociation of CH_3CHO in the presence of Ar collisions at 308 nm, enhancement of the low energy component of the CH_4 vibrational distribution evidences the TS pathway observation. The branching fractions of H-roaming, CH_3-roaming and TS contribution can be evaluated experimentally. The photodissociation of $HCOOCH_3$ at 248 nm yields the rovibrational energy disposal of CO up to v=4 and roaming appearance at v=1 and 2 with the current FTIR experiment, different from the molecular beam experiments yielding only the CO (v=1) fragment with some lower rotational levels. Thus, the roaming branching dependence on the vibrational states may be studied to find out any trend for the roaming behavior.

Acknowledgement

This work is supported by Ministry of Science and Technology of Taiwan, Republic of China under contract no. NSC 99-2113-M-002-010-MY3.

References

1. P. Carlier, H. Hannachi, and G. Mouvier, *Atmospheric Environment* 1986, **20**, 2079–2099.

2. A. Vairavamurthy, J. M. Roberts, and L. Newman, *Atmospheric Environment* 1992, **26A**, 1965–1993.

3. 1. J. H. Butler, M. Battle, M. L. Bender, S. A. Montzka, A. D. Clarke, E. S. Saltzman, C. M. Sucher, J. P. Severinghaus, and J. W. Elkins, *Nature* 1999, **399**, 749-755.

4.K. C. Lin and P. Y. Tsai, *Phys. Chem. Chem. Phys.* 2014, **16**, 7184-7198.

5. J. G. Calvert and J. N. Pitts, Jr., *Photochemistry* (Wiley, New York, 1966). Chap. 5.

6. S. Deshmukh and W. P. Hess, *J. Chem. Phys.* 1994, **100**, 6429-6433.

7. M. D. Person, P. W. Kash, and L. J. Butler, *J. Chem. Phys.* 1992, **97**, 355-373.

8. S. North, D. A. Blank, and Y. T. Lee, *Chem. Phys. Lett.* 1994, **224**, 38-42.

9. I. C. Lane, R. Meehan, and I. Powis, *J. Phys. Chem.* 1995, **99**, 12371-12374.

10. R. J. Horwitz, J. S. Fransisco, and J. A. Guest, *J. Phys. Chem. A* 1997, **101**, 1231-1237.

11. S. W. North, A. J. Marr, A. Furlan, and G. E. Hall, *J. Phys. Chem. A* 1997, **101**, 9224-9232.

12. J. C. Owrutsky and A. P. Baronavski, *J. Chem. Phys.* 1999, **111**, 7329-7336.

13. A. Furlan, H. A. Schels, and J. R. Huber, *J. Phys. Chem. A* 2000, **104**, 1920-1929.

14. I. R. Lee, Y. C. Chung, W. K. Chen, X. P. Hong, and P. Y. Cheng, *J. Chem. Phys.* 2001, **115**, 10656-10670.

15. M. C. Yoon, Y. S. Choi, and S. K. Kim, *J. Chem. Phys.* 1999, **110**, 7185-7191.

16. Y. Y. Yeh, M. H. Chao, P. Y. Tsai, Y. B. Chang, M. T. Tsai, and K. C. Lin, *J. Chem. Phys.* 2012, **136**, 044302.

17. Z. R. Wei, X. P. Zhang, W. B. Lee, B. Zhang, and K. C. Lin, *J. Chem. Phys.* 2009, **130**, 014307.

18. 20. L. R. McCunn, M. J. Krisch, K. Takematsu, L. J. Butler, and J. N. Shu, *J. Phys. Chem. A* 2004, **108**, 7889-7894.

19. P. R. Winter, B. Rowland, W. P. Hess, J. G. Radziszewski, M. R. Nimlos, and G. B. Ellison, *J. Phys. Chem. A* 1998, **102**, 3238-3248.

20. M. T. Tsai, Y. T. Liu, C. Y. Liu, P. Y. Tsai, and K. C. Lin, *Chem. Phys.*, 2010, **376**, 1-9.

21. C.-Y. Liu, M.-T. Tsai, P.-Y. Tsai, Y.-T. Liu, K. C. Lin, S. Y. Chen, and A. H. H. Chan, *ChemPhysChem.* 2011, **12**, 206-216.

22. E.-L. Hu, P.-Y. Tsai, H. Fan, and K.-C. Lin, *J. Chem. Phys.* 2013, **138**, 014302.

23. R. Sumathi and A. K. Chandra, *Chem. Phys.* 1994, **181**, 73-84.

24. M. M. Maricq and J. J. Szente, *Chem. Phys. Lett.* 1994, **220**, 243-250.

25. T. Shibata and T. Suzuki, *Chem. Phys. Lett.* 1996, **262**, 115-119.

26. E. Arunan, *J. Phys. Chem. A* 1997, **101**, 4838-4839.

27. B. Rowland and W. P. Hess, *J. Phys. Chem. A*, 1997, **101**, 8049-8056.

28. M. D. Person, P. W. Kash, and L. J. Butler, *J. Phys. Chem.* 1992, **96**, 2021-2023.

29. L. J. Butler, *Annu. Rev. Phys. Chem.* 1998, **49**, 125-171.

30. X. Tang, B. J. Ratliff, B. L. FitzPatrick, and L. J. Butler, *J. Phys. Chem. B* 2008, **112**, 16050-16058.

31. P. Ho, D. J. Bamford, R. J. Buss, Y. T. Lee, and C. B. Moore, *J. Chem. Phys.* 1982, **76**, 3630-3636.

32. H. Z. Li, Q. Li, W. T. Mao, Q. H. Zhu, and F. A. Kong, *J. Chem. Phys.*,1997, **106**, 5943-5946.

33. Y. T. Liu, M. T. Tsai, C. Y. Liu, P. Y. Tsai, and K. C. Lin, *J. Phys. Chem. A* 2010, **114**, 7275-7283.

34. J. Shi, T. J. Wallington, and E. W. Kaiser, *J. Phys. Chem.* 1993, **97***,* 6184-6192.

35. Y. Bedjanian, G. Laverdet, and G. Le Bras, *J. Phys. Chem. A* 1998, **102**, 953-959.

36. C. Vlnckier and W. Debruyn, *J. Phys. Chem.* 1979, **83**, 2057-2062.

37. H. M. Su, W. Mao, and F. Kong, *Chem. Phys. Lett.* 2000, **322**, 21-26.

38. G. Hancock and V. Haverd, *Chem. Phys. Lett.* 2003, **372**, 288-294.

39. J. I. Aoyama, T. Sugihara, K. Tabayashi, and K. Saito, *J. Chem. Phys.* 2003, **118**, 6348-6357.

40. S.P. SO, *Chem. Phys. Lett.* 1997, **270**, 363-368.

41. W. H. Fang, R. Z. Liu, and X. Z. You, *Chem. Phys. Lett.* 1994, **226**, 453-458.

42. R. Sumathi and M. T. Nguyen, *J. Phys. Chem. A* 1998, **102**, 412-421.

43. P.-Y. Tsai and K.-C. Lin, *J. Chem. Phys.* 2013, **138**, 246102.

44. C. Wittig, I. Nadler, H. Reisler, M. Noble, J. Catanzarite, and G. Radhakrishnan, *J. Chem. Phys.* 1985, **83**, 5581-5588.

45. M. Hunter, S. A. Reid, D. C. Robie, and H. Reisler, *J. Chem. Phys.* 1993, **99**, 1093-1108.

46. J. T. Muckerman, *J. Phys. Chem.* 1989, **93**,179-184.

47. D. J. Donaldson and S. R. Leone, *J. Chem. Phys.* 1986, **85**, 817-824.

48. V. Horka, S. Civis, V. Špirko, and K. Kawaguchi, *Collect. Czech. Chem. Commun.* 2004, **69**, 73-89.

49. S. Nagata, T. Yamabe, and K. Fukui, *J. Phys. Chem*. 1975, **79**, 2335-2340.

50. R. M. Romano, C. O. Della Védova, and A. J. Downs, *J. Phys. Chem. A* 2002, **106**, 7235-7244.

51. A. M. Lu, M. Ke, W. J. Ding, and R Z. Liu, *Chin. J. Chem.* 2009, **27**, 227-234.

52. Gestion et Etude des Informations Spectroscopiques Atmosphériques (GEISA) spectroscopic database, 2003 edition.

53. P. E. B. Butler, D. R. Eaton, and H. W. Thompson, *Spectrochim. Acta*, 1958, **13**, 223-235.

54. L. Lechuga-Fossat, J.-M. Flaud, C. Camy-Peyret, and J. W. C. Johns, *Can. J. Phys.* 1984, **62**, 1889-1894.

55. R. Warmbier, R. Schneider, A. R. Sharma, B. J. Braams, J. M. Bowman, and P. H. Hauschildt, *Astron & Astrophys.* 2009, **495**, 655-661.

56. R. D. van Zee, M. F. Foltz, and C. B. Moore, *J. Chem. Phys.* 1993, **99**, 1664-1673.

57. A. Suits, *Acc. Chem. Res.* 2008, **41**, 873-881.

58. J. M. Bowman and B. C. Shepler, *Annu. Rev. Phys. Chem.* 2011, **62**, 531-553.

59. K. L. K. Lee, M. S. Quinn, A. T. Maccarone, K. Nauta, P. L. Houston, S. A. Reid, M. J. T. Jordan, and S. H. Kable, *Chem. Sci.* 2014, **5**, 4633-4638. (and references therein)

60. B. R. Heazlewood, M. J. T. Jordan, S. H. Kable, T. M. Selby, D. L. Osborn, B. C. Shepler, B. J. Braams, and J. M. Bowman, *Proc. Nat. Acad. Sci. USA* 2008, **105**,

12719-12724.

61. P. L. Houston and S. H. Kable, *Proc. Natl. Acad. Sci. USA* 2006, **103**, 16079-16082.
62. L. Rubio-Lago, G. A. Amaral, A. Arregui, J. G. Izquierdo, F. Wang, D. Zaouris, T. N. Kitsopoulos, and L. Banares, *Phys. Chem. Chem. Phys.* 2007, **9**, 6123-6127.
63. L. Rubio-Lago, G. A. Amaral, A. Arregui, J. Gonzalez-Vazquez, and L. Banares, *Phys. Chem. Chem. Phys.* 2012, **14**, 6067-6078.
64. B. C. Shepler, Y. Han, and J. M. Bowman, *J. Phys. Chem. Lett.* 2011, **2**, 834-838.
65. H-K. Li, P-Y. Tsai, K-C. Hung, T. Kasai, and K-C. Lin, *J. Chem. Phys.* 2015, **142**, 041101.
66. P.-Y. Tsai, K.-C. Hung, H.-K. Li, and K.-C. Lin, *J. Phys. Chem. Lett.* 2014, **5**, 190-195.
67. K–C. Hung, P.-Y. Tsai, H.-K. Li, and K.-C. Lin, *J. Chem. Phys.* 2014, **140**, 064313.
68. National Institute of Standards and Technology, *NIST Chemical Kinetics Database* (http://kinetics.nist.gov/kinetics/index.jsp)
69. M. A. Barteau and R. J.Madix, *J. Catal.,* 1980, **62**, 329-340.
70. F. Q. Ma, D. S. Lu, and Z. Y. Guo, *J. Mol. Catal.,* 1993, **78**, 309-318.
71. S. H. Lee, *J. Chem. Phys.* 2008, **129**, 194304.
72. M.-H. Chao, P.-Y. Tsai, and K.-C. Lin, *Phys. Chem. Chem. Phys.* 2011, **13**, 7154-7161.
73. P. Y. Tsai, M. H. Chao, T. Kasai, K. C. Lin, A. Lombardi, F. Palazzetti, and V. Aquilanti, *Phys. Chem. Chem. Phys.* 2014, **16**, 2854-2865.
74. G. Cui, F. Zhang, and W. Fang, *J Chem. Phys.* 2010, **132**, 034306.
75. M. Nakamura, P. Y. Tsai, T. Kasai, K. C. Lin, F. Palazzetti, A. Lombardi, and V. Aquilanti, *Faraday Discussion*, 2015, **177**, 77-98.

76. T. Carrington, Jr., L. M. Hubbard, H. F. Schaefer III, and W. H. Miller, *J. Chem. Phys.* 1984, **80**, 4347-4354.

77. B. Li and W. Bian, *J. Chem. Phys.* 2008, **129**, 024111.

78. J. Levin, H. Feldman, A. Baer, D. Ben-Hamu, O. Heber, D. Zajfman, and Z. Vager, *Phys. Rev. Lett* 1998. **81**, 3347-3350.

79. P-W. Lee, P. G. Scrape, L. J. Butler, and Y.-P. Lee, *J. Phys. Chem. A*, 2015, **119**, 7293-7304.

80. N. Pietri, M. Monnier and J.-P. Aycard, *J. Org. Chem.*, 1998, **63**, 2462-2468.

81. G. A. Amaral, A. Arregui, L. Rubio-Lago, J. D. Rodriguez, and L. Banares, *J. Chem. Phys.* 2010, **133**, 064303.

82. B. R. Heazlewood, S. J. Rowling, A. T. Maccarone, M. J. T. Jordan, and S. H. Kable, *J. Chem. Phys.* 2009, **130**, 054310.

83. B. R.Heazlewood, A. T. Maccarone, D. U. Andrews, D. L. Osborn, L. B. Harding, S. J. Klippenstein, M. J. T. Jordan, and S. H. Kable, *Nature Chemistry* 2001, **3**, 443-448.

84. B. F. Gherman, R. A. Friesner, T.-H. Wong, Z. Min, and R. Bersohn, *J. Chem. Phys.* 2001, **114**, 6128-6133.

85. B. Fu, Y. Han, and J. M. Bowman, *Faraday Discuss.* 2012, **157**, 27-39.

Figure Captions

Fig.1 Pressure dependence of low-resolution emission spectra of CO (left, 1900-3200 cm^{-1}) and HCl (right, 2200-3200 cm^{-1}) appearing in the region of 1950-2250 cm^{-1} and 2400-3200 cm^{-1}, respectively, in the presence of Ar at 30 μs delay following photolysis of CH_3COCl at 248 nm.

Fig.2 (a)Time-dependence of the CO_2 appearance from a reaction of CH_2 with O_2, in which CH_2 is decomposed from the CH_2CO moiety generated in photolysis of CH_3COCl at 248 nm. (b)The linear fit yields a production rate constant of

(2.1±0.2) x 10^{-12} cm^3/molecule.s based on the formula, $ln([CO_2]_{max} - [CO_2]) = ln[CO_2]_{max} - k't$ and $k'=k[O_2]$ in which the O_2 pressure is 1200 mTorr (ref.33).

Fig.3 The dissociation channels of CH_3COCl, in which the energies in kcal/mol relative to the ground state are computed with CCSD(T)/cc-pVTZ level of theory with B3LYP/6-311G(d,p) zero-point energy corrections at B3LYP/6-311G(d,p) optimized geometries. For those pathways with dashed line, the attempts for locating the transition states are not made or not successful.

Fig.4 (a) High-resolution spectra of HCN (left) and CO (right) as a function of the μs delay time in the photolysis of CH_3COCN in the presence of Ar at 2000 and 1200 mTorr, respectively. The number in the top left inset indicates the μs delay time with respect to the laser firing.

(b) The HCN emission spectra with spectral resolution of 0.5 cm^{-1} acquired in the range of 3100-3400 cm^{-1} at 4 μs delay after photolysis in the presence of Ar at 2000 mTorr. The HNC emission spectra can be recognized in the range of 3450 - 3700 cm^{-1}, but cannot be assigned precisely.

Fig.5 (a) Dissociation pathway of CH_3COCN via isomerization transition state.

(b) Prior distributions of CO calculated for a primary channel, CO + CH_3NC, and a three-body dissociation, CH_2+CO+HCN, in comparison with the observed results.

Fig.6 The Ar pressure dependence of the HCN area intensity over the low-resolution spectra obtained at 4 μs delay in photolysis of CH_3COCN at

308 nm. According to the equations in ref.(16), the experimental data are fitted to yield the optimized rate constants for the collision-induced internal conversion.

Fig.7 Population decay of OCS(v_3) and $CH_2CO(v_2)$ in the 1950–2080 and 2100–2200 cm^{-1} region, respectively, after 10 μs delay in photolysis of CH_3COSH at 248 nm. OCS starts from v = 6 at 1957 cm^{-1}, relaxes toward low v, and finally vanishes after 280 μs delay. $CH_2CO(v_2)$ at 2150 cm^{-1} having partial overlap with OCS seems to decay downward.

Fig.8 Identification of CH_3SH, CH_4, and H_2S in the 2400-3300 cm^{-1} region in photolysis of CH_3COSH at 248 nm. The spectral region contains three profiles at about 2590, 2920, and 3000 cm^{-1}. $CH_3SH(v_3)$ and $H_2S(v_1,v_3)$ contribute to the first region, $CH_3SH(v_2)$ dominates the second one, while $CH_4(v_3)$ dominates the third one.

Fig.9 (a) Three dissociation pathways of CH_3COSH on the ground state surface were computed previously using hybrid density functional theory B3LYP with cc-pVTZ and other basis sets.

(b)Vibrational population of CO product obtained by (1) experimental observation, (2) prior distribution of $CH_2 + H_2S + CO$, and (3) prior distribution of $CH_3SH + CO$. Population of CO(v=1) is normalized for comparison.

Fig.10 (a) CO emission spectra (1900- 2200 cm^{-1}) with a spectral resolution of 0.25 cm^{-1} in 7 μs delay after photolysis of CH_3CHO at 308 nm in the

presence of Ar at 3000 mTorr. The corresponding spectral simulation is included for comparison.

(b) Deconvolution of two Boltzmann rotational distributions of CO at v=1, yielding a ratio of 10% to 90% for the low-J and high-J component.

Fig.11 (a) CH_4 vibrational energy distribution (binned at 1500 cm^{-1} interval) extracted from the ro-vibrational spectrum observed in photolysis of CH_3CHO at 308 nm.

(b) A single-modal CH_4 vibrational distribution was observed using similar time-resolved FTIR emission spectroscopy (see ref.60). The experimental result is consistent with the QCT calculations performed on the global minimum configuration of the PES. However, the QCT calculations performed on the transition state configuration result in a small energy component that was not found in the experiments.

Fig.12 Energy scheme for H-roaming, CH_3-roaming and transition state pathways in photolysis of CH_3CHO at 308 nm. The CO vibrational states are denoted with a harmonic frequency of 1800 cm^{-1} obtained from the CO stretch mode of CH_3CO structure, because the incipient H + CH_3CO radicals are expected to be close to the nascent CO product via the H-roaming.

Fig.13 A schematic view of the photodissociation pathways of methyl formate. The minimum energy path, from the ground state to the dissociated products CH_3OH + CO passing through the transition state, is represented by the red-dashed line. The molecule in the ground state (S_0) is promoted to

the excited state (S_1) at 248 nm. The very large vibronic coupling induces the transition to the ground state through the conical intersection giving CH_3OH + CO products, while the triple dissociation channel, CH_3O + CO + H, is not accessible because its threshold is slightly higher than the energy provided by the laser.

Fig.14 The images (left panel) and the extracted kinetic energy distributions of vibrational excited CO (v=1) from photodissociation of methyl formate at 248 nm, for the selected rotational levels J = 2, 7, and 11. In the central panels, fits of the experimental data (green curve) and deconvolution of the slow (in blue) and fast (in red) components are reported. Panels on the right-hand side show the corresponding results as obtained by classical trajectory simulations.

Fig.15 The CO vibrational population from v=1 to 4 extracted in the spectral range from 2000 to 2150 cm^{-1} in photolysis of methyl formate at 248 nm. The bimodal rotational distributions are obtained for v = 1 and 2, while a single-peaked distribution for v=3 and 4. The Boltzmann rotational temperatures are characterized.

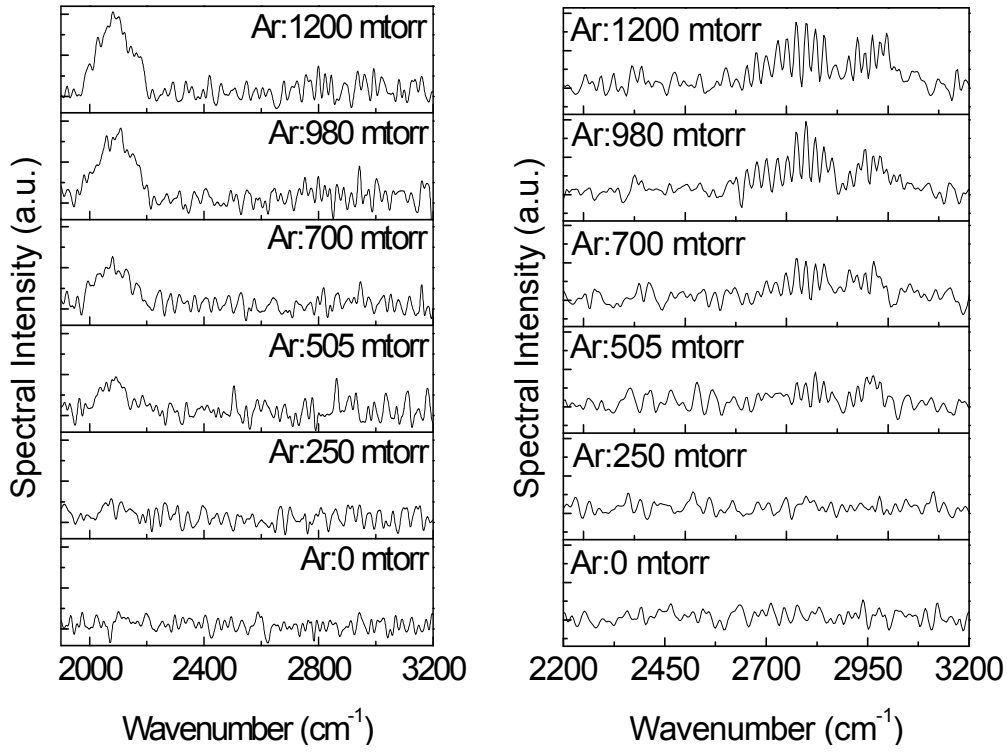

Fig.1

(a)

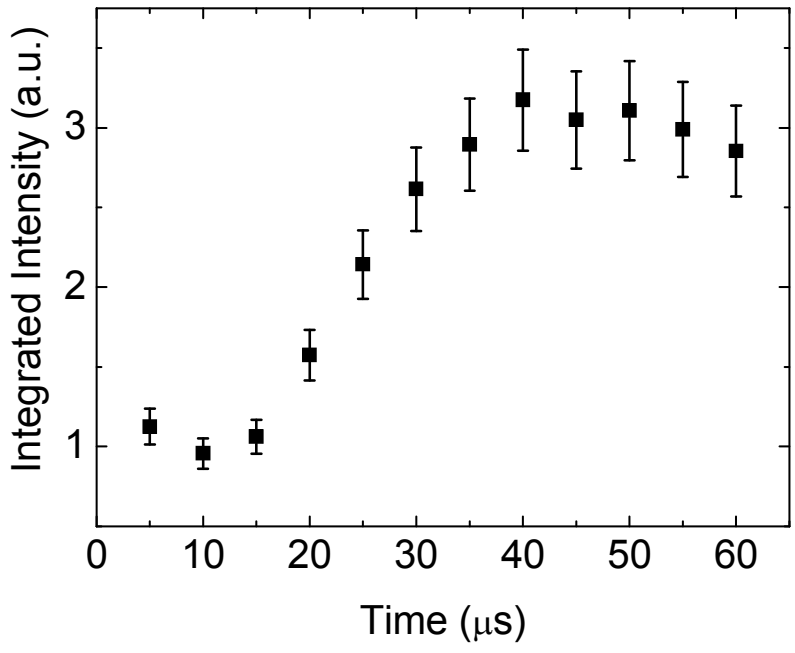

(b)

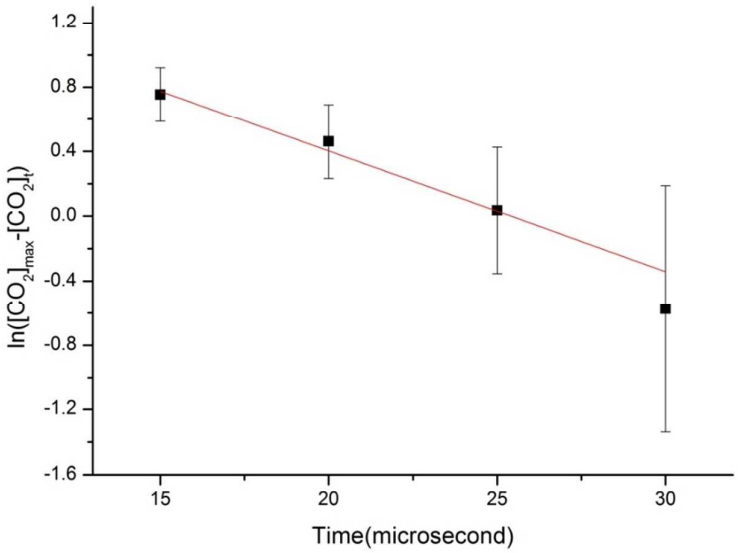

Fig.2

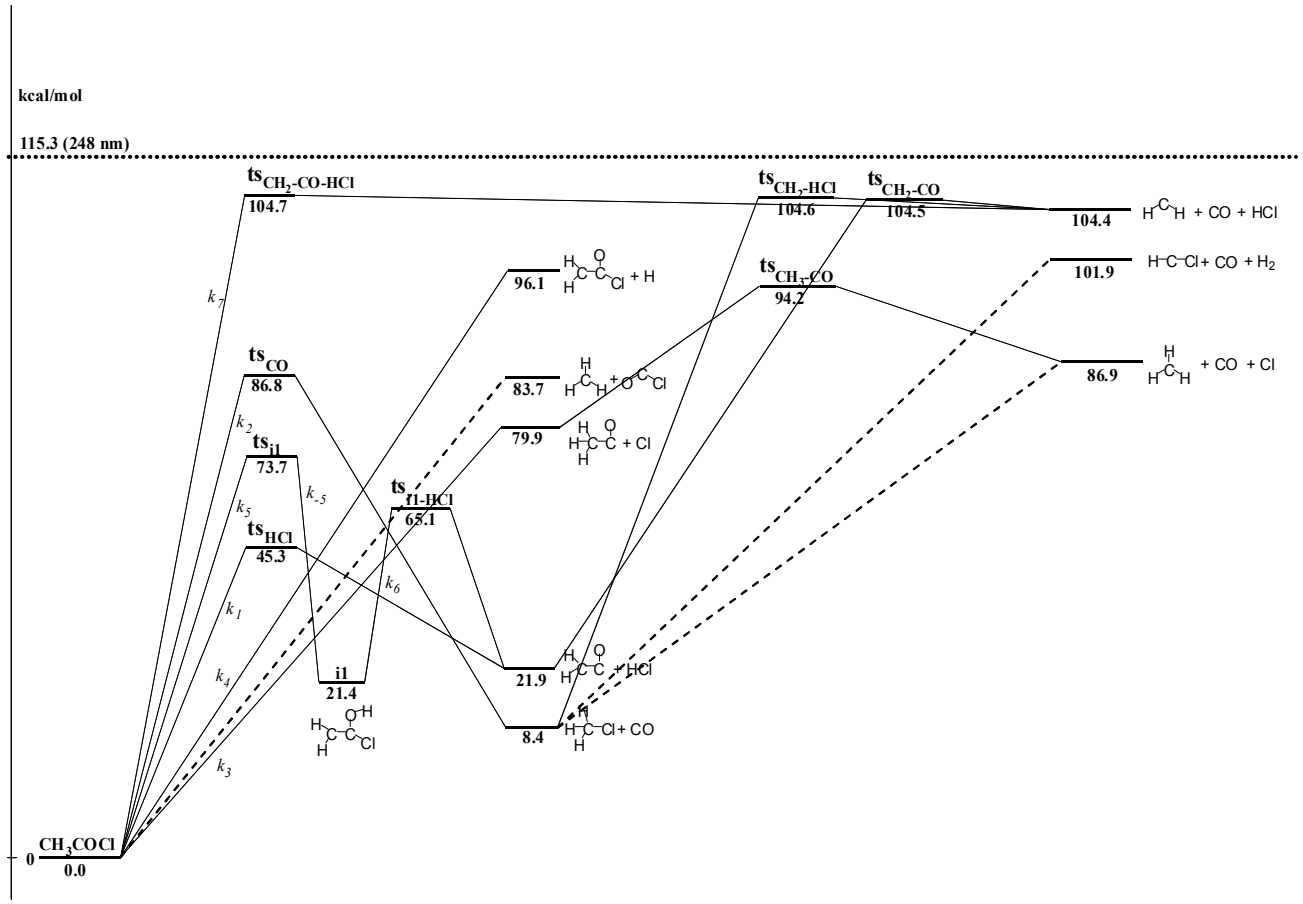

Fig.3

(a)

HCN **CO**

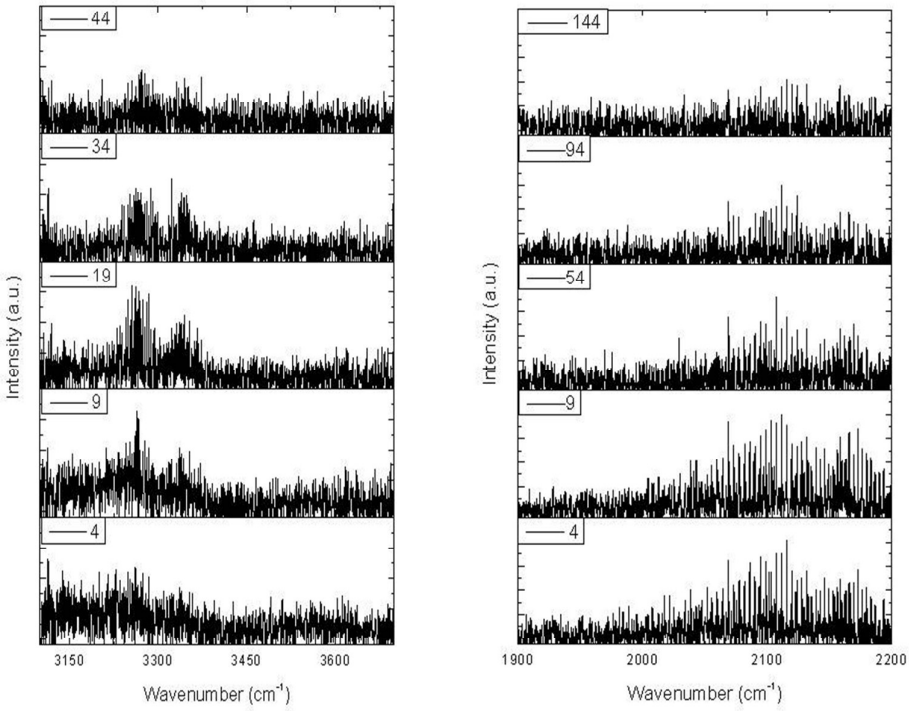

(b)

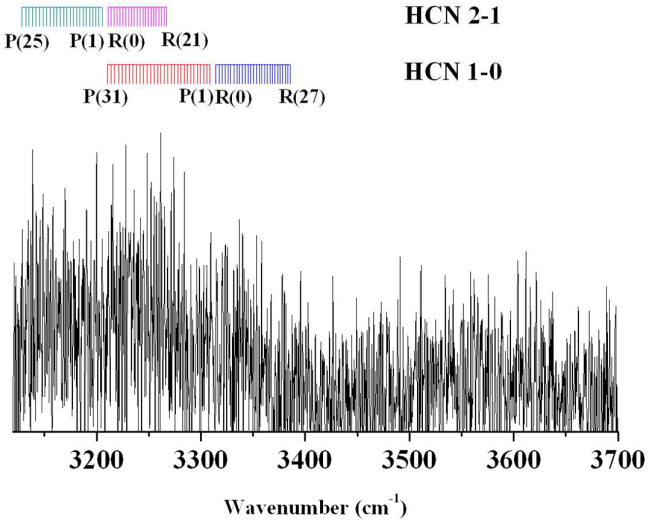

Fig.4

(a)

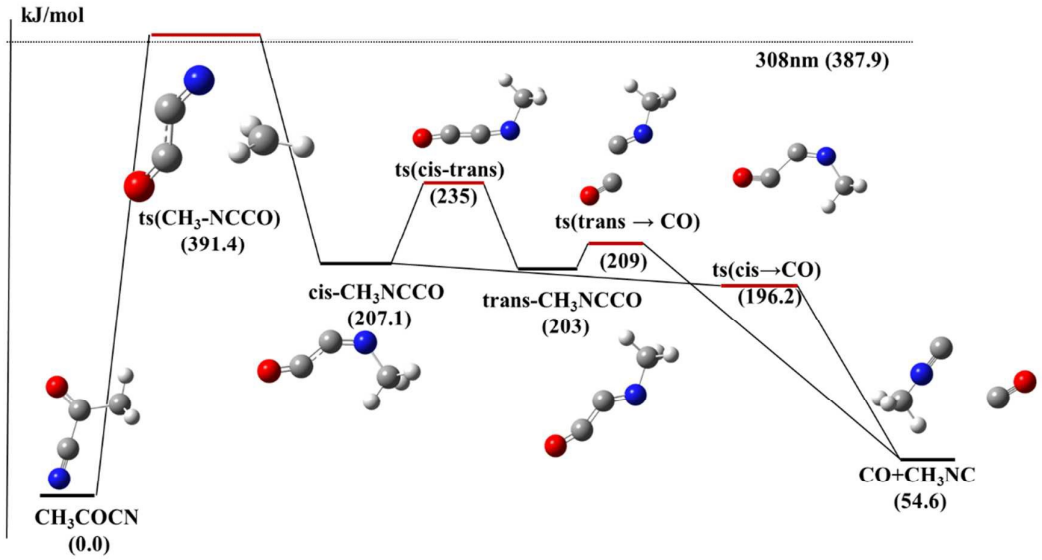

(b)

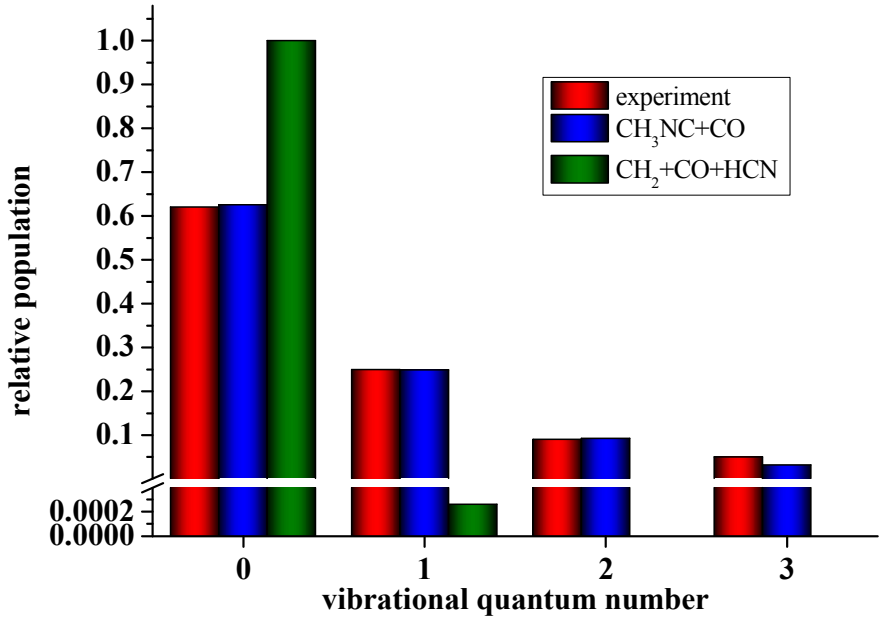

Fig.5

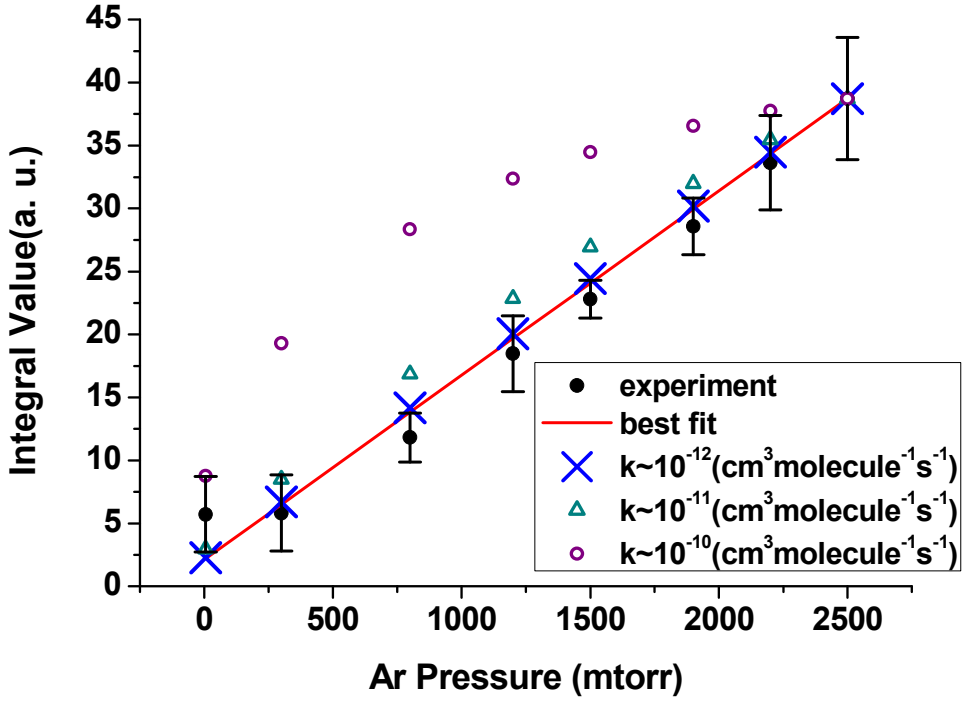

Fig.6

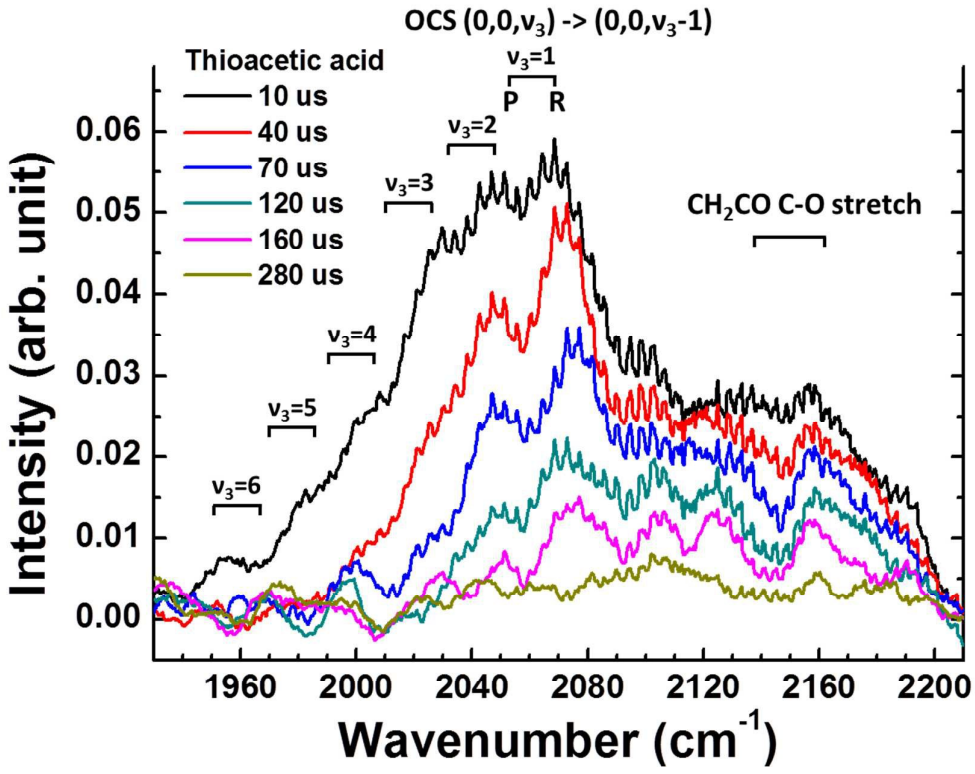

Fig.7

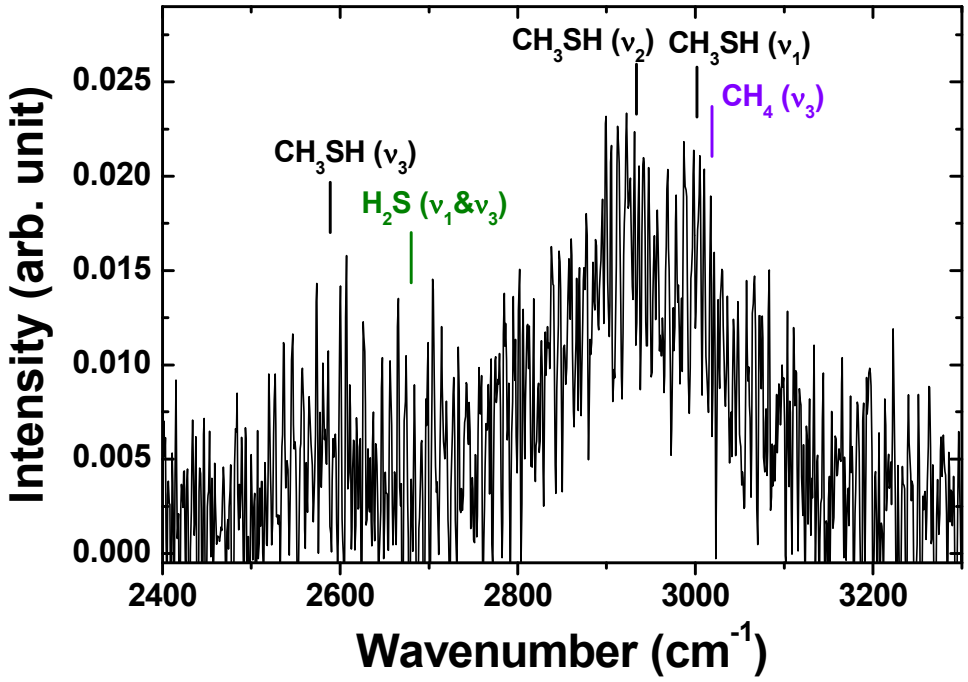

Fig.8

(a)

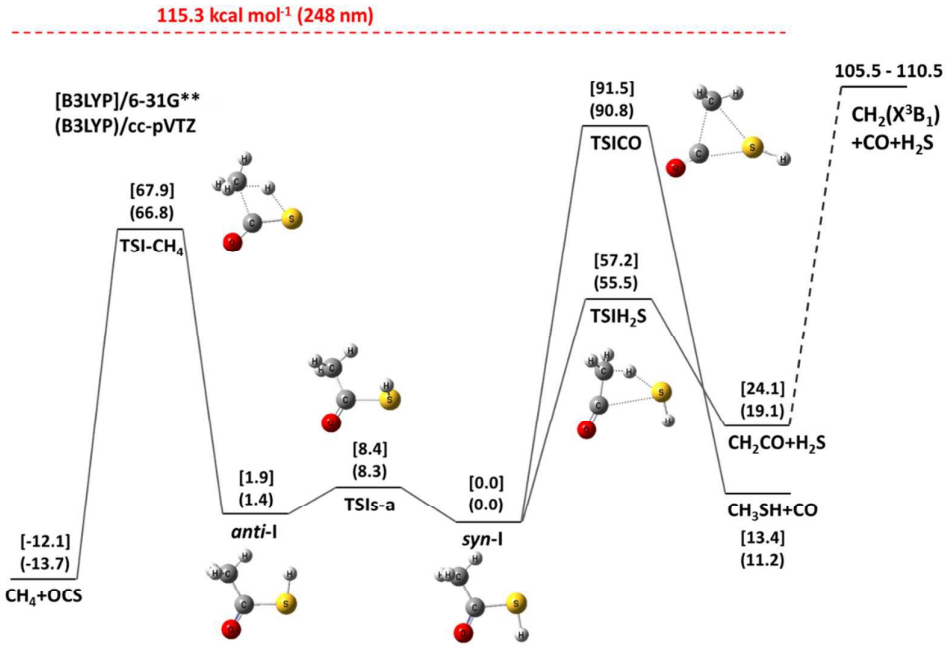

(b)

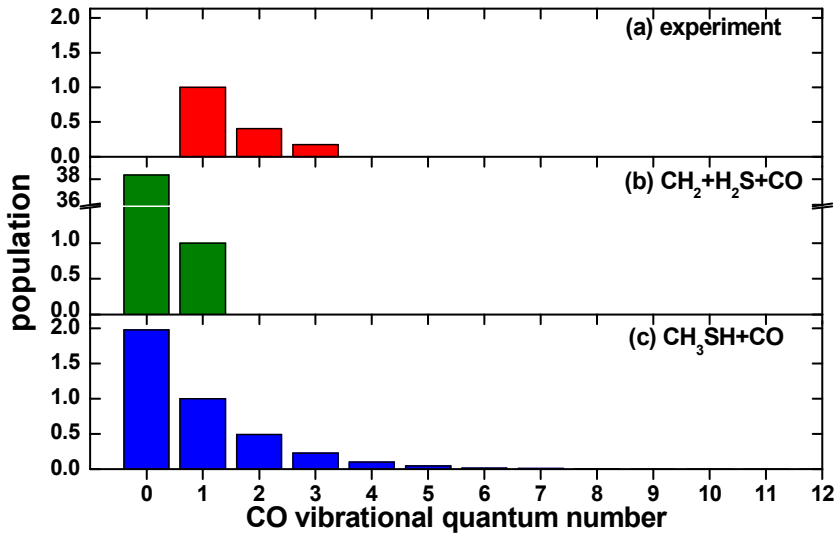

Fig.9

(a)

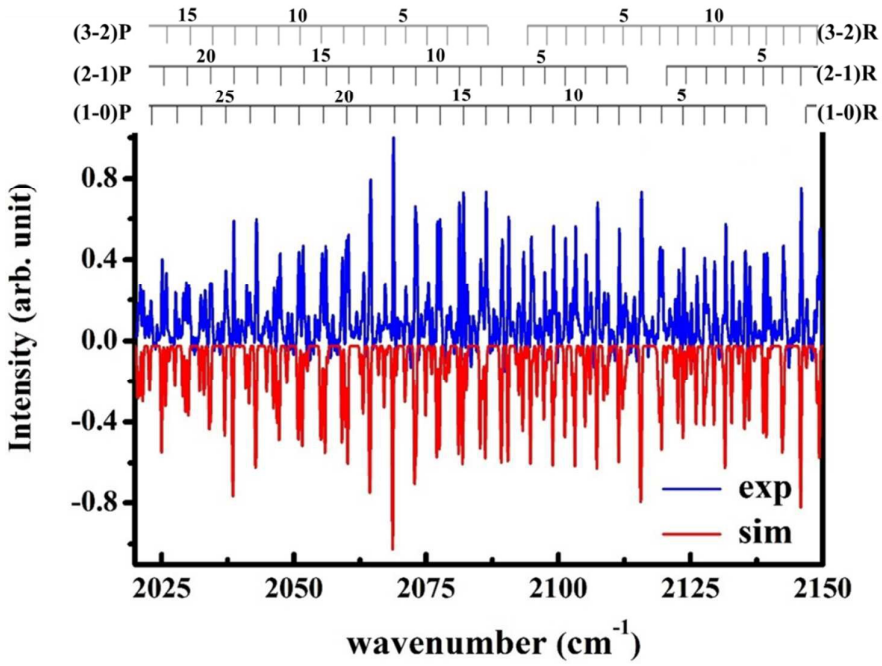

(b)

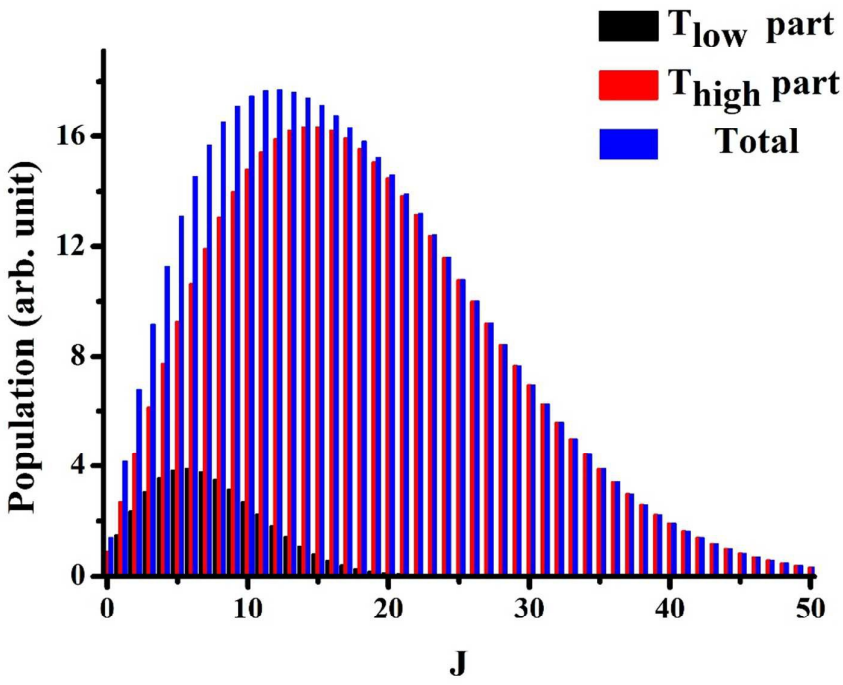

Fig.10

(a)

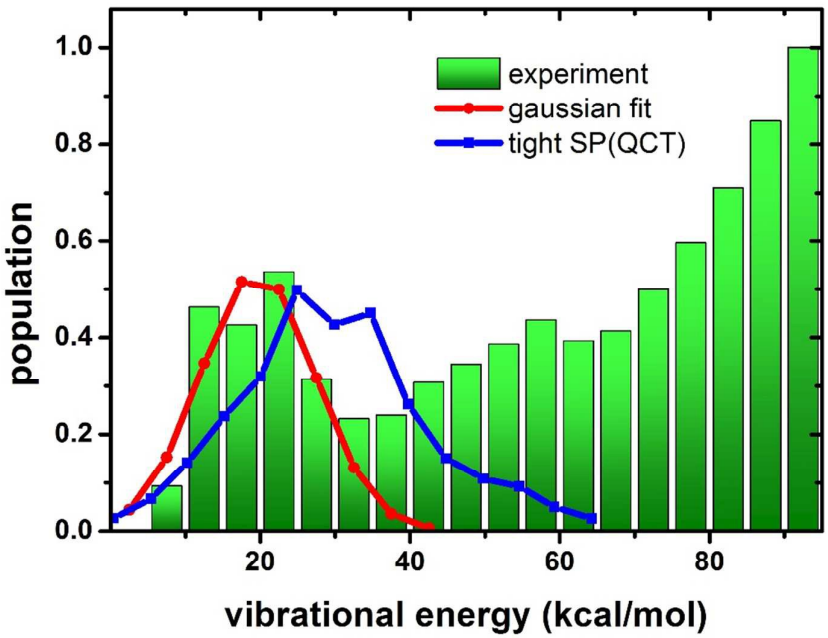

(b)

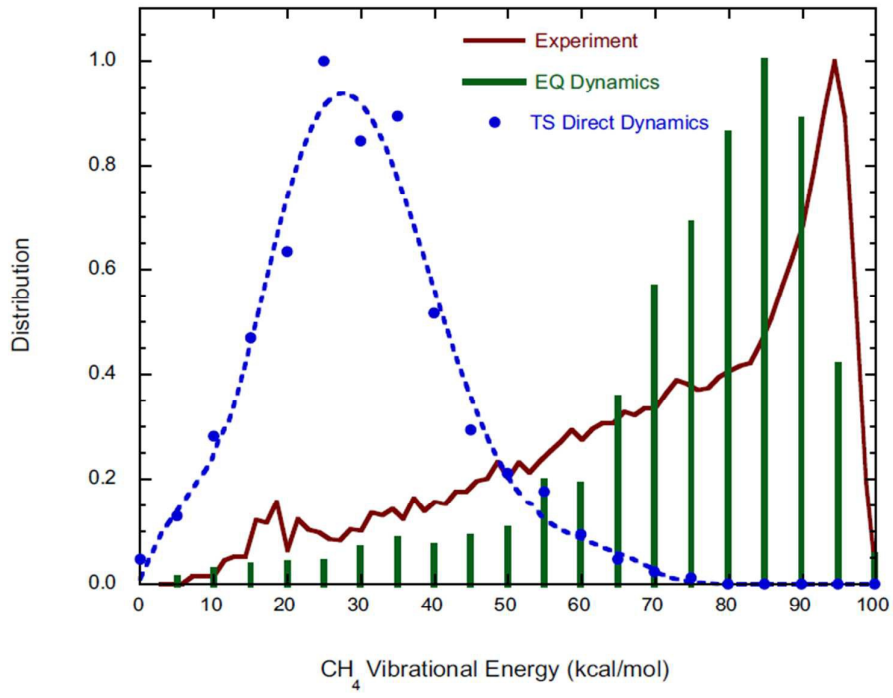

Fig.11

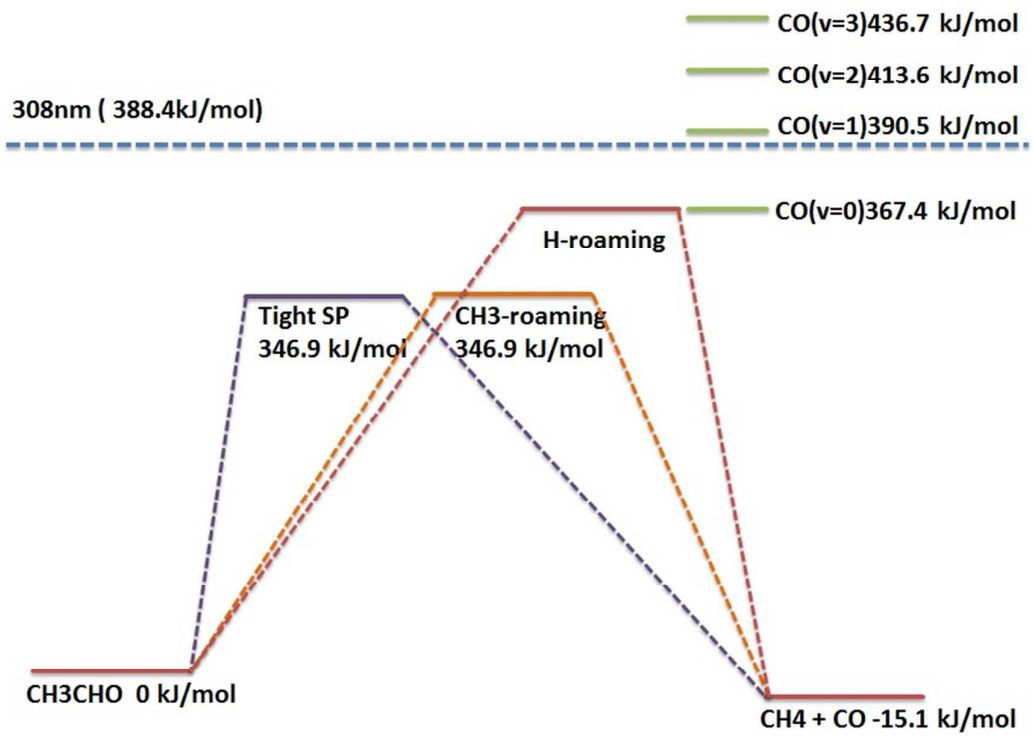

Fig.12

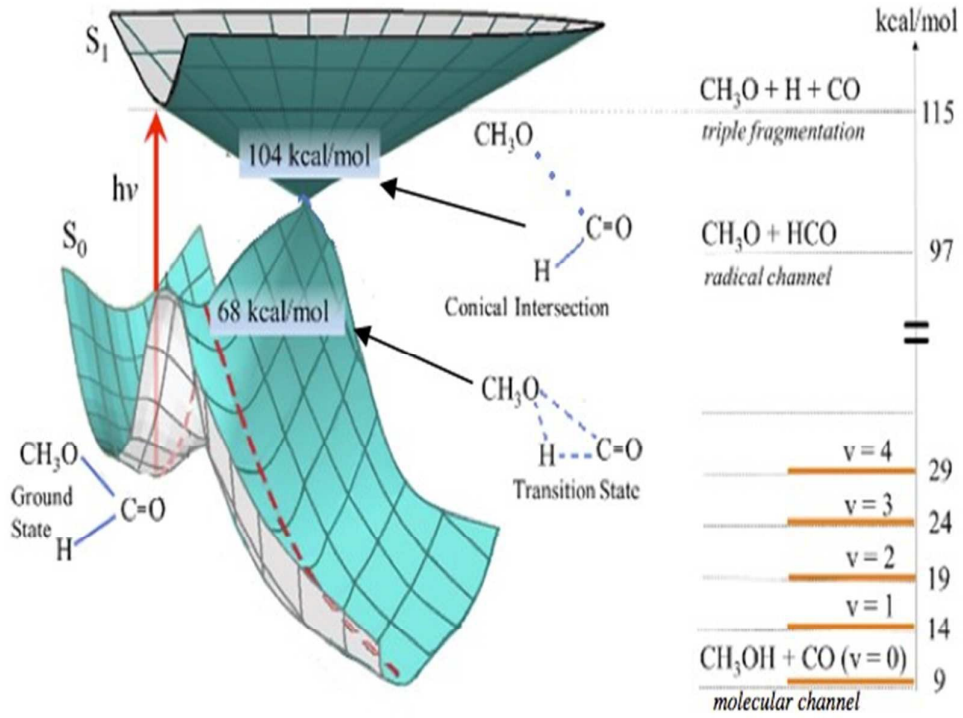

Fig.13

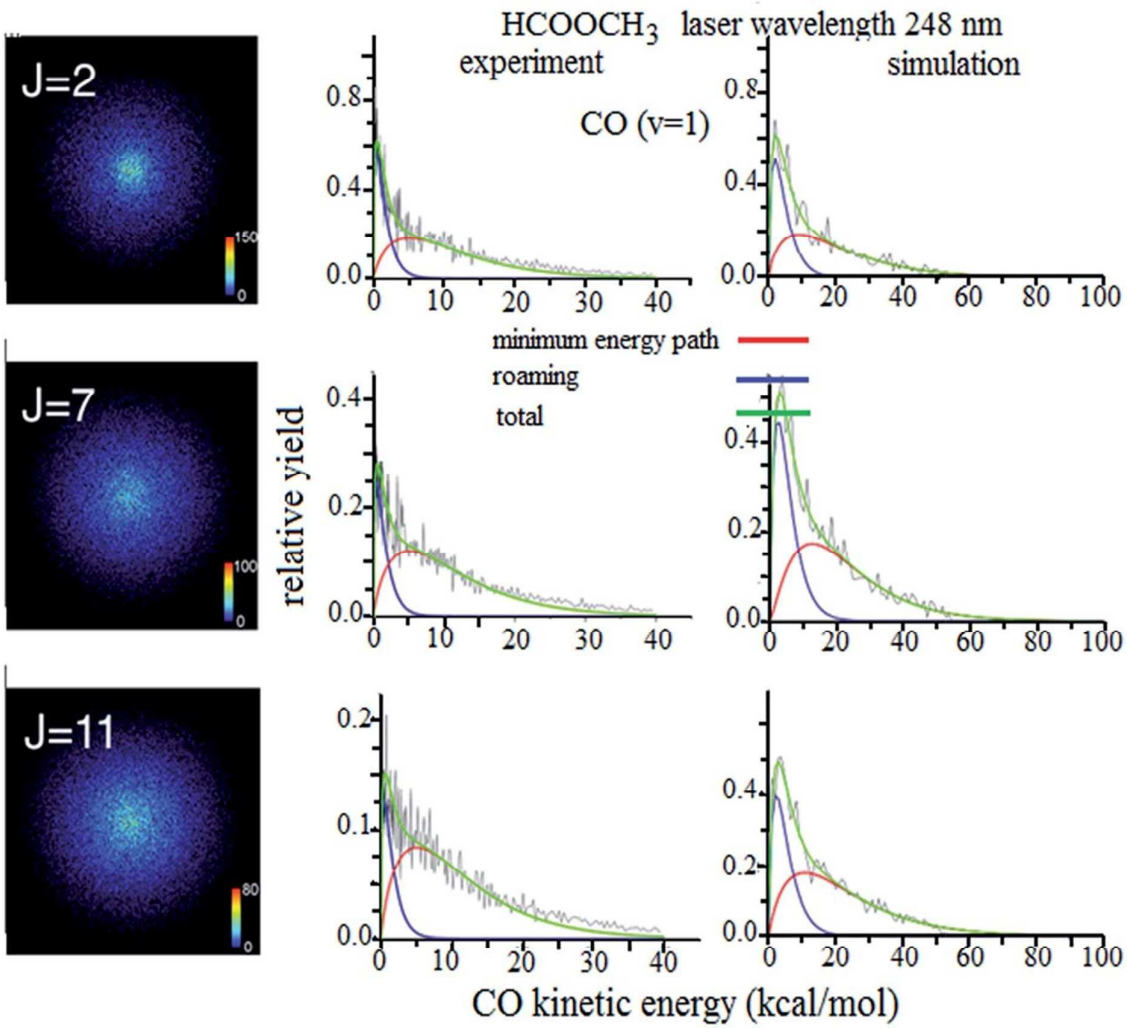

Fig.14

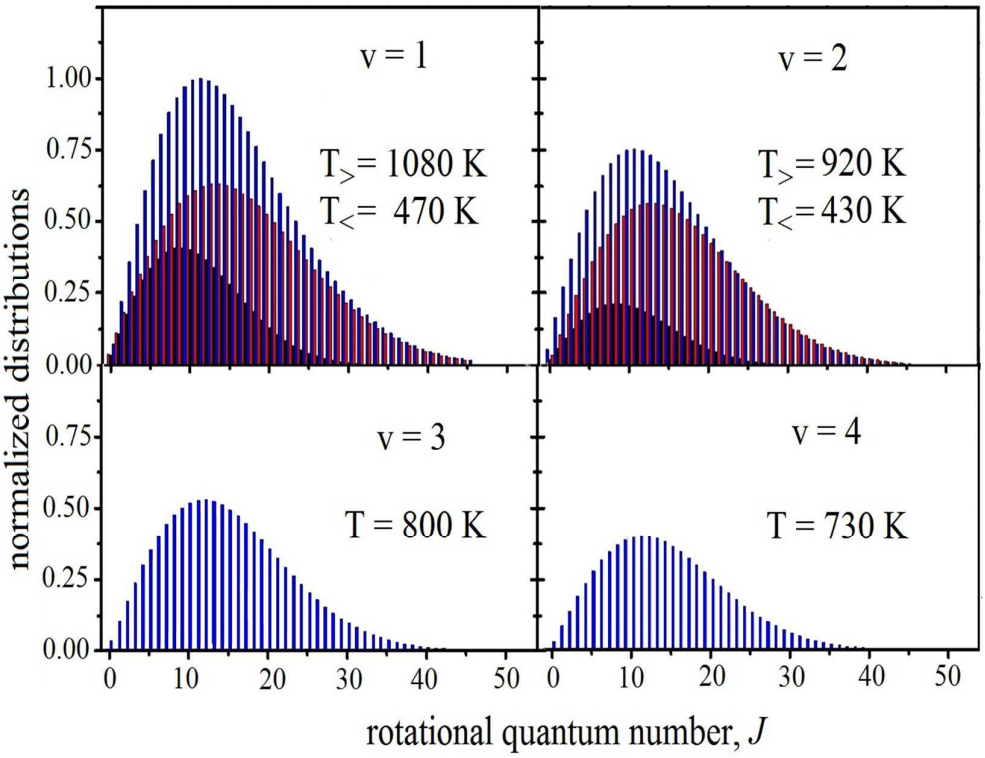

Fig.15

Biographic Information

King-Chuen Lin is a Distinguished Professor of the Department of Chemistry at National Taiwan University and a Distinguished Research Fellow of National Science Council, Taiwan. He received his B.S. degree in Chemistry from National Taiwan University, Taiwan, his PhD in Chemistry from Michigan State University, USA, and his postdoctoral career at Cornell University. His research interests are photodissociation and reaction dynamics in gas and condensed phases, atmospheric chemistry, and single molecule spectroscopy.